5-1-2002

Anisotropic-Reflectance Correction of Multispectral Satellite Imagery in Complex Mountain Terrain

Stephen B. Cacioppo
University of Nebraska at Omaha

Anisotropic-Reflectance Correction of Multispectral Satellite Imagery in Complex Mountain Terrain

A Thesis

Presented to the

Department of Geography-Geology

and the

Faculty of the Graduate College

University of Nebraska

In Partial Fulfillment

Of the Requirements for the Degree

Master of Arts

University of Nebraska at Omaha

By

Stephen B. Cacioppo

May, 2002

THESIS ACCEPTANCE

Acceptance for the faculty of the Graduate College,

University of Nebraska, in partial fulfillment of the

requirements for the degree Master of Arts,

University of Nebraska at Omaha.

Committee

Michael P. Bishop 4/17/02

Chairperson: Dr. Michael P. Bishop Date
Department of Geography/Geology

John F. Shroder, Jr. 17/4/02

Committee Member: Dr. Jack F. Shroder, Jr. Date
Department of Geography/Geology

Betty L Hickman 4-17-02

Committee Member: Dr. Betty L. Hickman Date
Department of Mathematics

Acknowledgements

No one person develops wholly on his own. As with most projects, this thesis would not have been possible without the support, motivation and inspiration of many people. For those who said this thesis could not be done, thank you. You gave me motivation and I'm proud of my accomplishment.

I am grateful to Dr. John F. Shroder Jr. and Dr. Betty L. Hickman for serving on my thesis committee. To Jeff Olsenholler, a special thanks for my nickname, and for your encouraging, positive re-enforcing attitude. To Dr. Michael P. Bishop, I appreciate your patience, assistance, enthusiasm, and drive for excellence, pushing me when sometimes I would have done otherwise.

To my father, who helped me "stay the course" and for his support and understanding of the task that I was undertaking no matter how upset or frustrated I became.

Finally, I would like to thank my wife Megan who encouraged and showed me how to become as committed to learning as she is.

Contents

List of Figures

List of Tables

Abstract

The utilization of satellite imagery acquired over rugged terrain is problematic because of anisotropic reflectance. A variety of environmental factors, such as the atmosphere and the topography, cause significant variation in the irradiant and radiant flux. Consequently, satellite imagery must be radiometrically corrected to account for these variations which influence the at-satellite spectral response. In mountain terrain, the topographic effect is very pronounced, and satellite imagery must be normalized utilizing various techniques. The purpose of this research was to evaluate various implementations of the Minnaert correction technique which were designed to account for the influence of topography and land cover on sensor response. Specifically, a local and land cover stratification procedure was developed and tested to compute multiple Minnaert constants. SPOT HRV satellite imagery of the Nanga Parbat Himalaya was used because the topography is extreme, and the study area represents an excellent location for testing anisotropic-reflectance correction procedures.

The SPOT-3 NIR image was used in the analysis as the atmospheric influence was minimal. A digital elevation model (DEM) was generated using SPOT-3 panchromatic stereopairs. The DEM was used to produce estimates of slope and slope aspect for accounting for variations in the local direct irradiant flux. Four subimages were selected to evaluate the spectral variance for two homogeneous areas and two heterogeneous areas. Effective anisotropic-reflectance correction should result in a decrease in spectral variation over homogeneous land cover and increased spectral variation among heterogeneous land

cover areas. Descriptive statistics and semivariogram analysis was used for evaluation of the original and normalized images.

Results indicated that the Cosine-correction method produced high radiance values throughout the image regardless of land cover. This over-correction was found wherever there were steep slopes, and is the result of not accounting for the correct magnitude of the surface irradiance. The Minnaert-correction procedure, using a global Minnaert constant, appeared to produce better results, however, global-regression analysis revealed results that did not accurately characterize the degree of anistropy for various land cover classes. Minnaert correction based upon land-cover stratification produced statistically valid results, such that both topography and land cover effects on the radiant flux were generally accounted for. The window-based approach produced images that appeared to reduce the topographic effect, although overcorrection still occurred, and statistical results were invalid for small window sizes. These results indicated that the Minnaert-Correction procedure has the potential to be used to reduce the topographic effect in rugged terrain, if scale-dependent variation in the topography and land-cover characteristics can be locally evaluated to compute Minnaert constants. Furthermore, the diffuse-irradiant and adjacent-terrain irradiant flux need to be considered as overcorrection is problematic in complex terrain. More research on dynamic spatial-partitioning of the topography and spectral variation is therefore warrented.

1 Introduction

Global climate models predict that the Earth's atmosphere may be getting warmer (Allen et al., 2000; Delworth and Knutson, 2000; Latif et al., 2000; Przybylak, 2000; Watterson, 2000). This would have an impact on atmospheric circulation and precipitation (Leung and Wigmosta, 1999; Dehn and Buma, 1999; Levi et al., 1999; Wild and Ohmura, 2000), ecosystems (Kirilenko et al., 2000), land cover (Kirilenko et al., 2000; Levi et al., 1999), and a variety of surface processes (Greuell and de Wildt, 1999; Jin and Simpson, 1999; Shroder et al., 1999). Physical evidence of global environmental change includes changes in sea level (Dowdeswell et al., 1997; Osterhus and Gammelsrod, 1999; Wild and Ohmura, 2000; Wu et al., 1999), ecotone and ecosystem migration (Kirilenko et al., 2000; Levi et al., 1999), and negative glacier mass balance (Dowdeswell, 1995; Dowdeswell et al., 1997; Dyurgerov and Meier, 1999; Vinnikov et al., 1999; Wild and Ohmura, 2000). Mountain environments are known to be sensitive to climatic fluctuations, therefore, scientists need to study these environments and monitor change caused by climate forcing. Because alpine environments are the result of the coupling of climate, surface processes and tectonics, they represent excellent laboratories for studying process dynamics and feedback mechanisms.

It is particularly difficult, however, to quantitatively assess and monitor complex mountain systems, given their spatial and temporal complexity (Bishop et al., 1998a). Information regarding land cover, topography, and process dynamics are required to effectively determine whether environmental change is the result of natural or anthropogenic factors. Field observations have been used to collect data, although traditional approaches are in-

adequate in terms of systematically characterizing the spatial and temporal variability of phenomena (Bishop et al., 1995, 1998b,a). Geographic Information System (GIS) technology provides new opportunities for scientists to study lithospheric processes and global environmental change (Bishop et al., 1998b; Dozier and Frew, 1990; Duguay and LeDrew, 1992; Jin and Simpson, 1999).

Perhaps the most significant advantage of GIS for studying mountain environments is the ability to characterize and model the spatial and temporal dependencies of biophysical variables, surface features, and process dynamics (Bishop et al., 1998b,a; Conese et al., 1993a; Ekstrand, 1996; Meyer et al., 1993). With the advent of advanced sensor systems and high resolution multispectral satellite imagery, scientists can now examine spatial patterns of landscape structure and process (Allen and Walsh, 1996; Jin and Simpson, 1999).

In order to systematically study complex processes in mountain environments, researchers must first be able to determine what environmental factors influence spectral reflectance. Spectral reflectance from a surface, as measured by a satellite, is influenced by a multitude of factors including:

- Atmospheric processes which include, attenuation, scattering, reflection, absorption and refraction (Hugli and Frei, 1983; Jin and Simpson, 1999; MacFarlane and Robinson, 1984).

- Numerous topographic parameters such as elevation, relief, slope and slope aspect. These parameters also influence atmospheric and landscape variables such that positive and negative feedback relationships must be considered (Conese et al., 1993a;

Dozier and Frew, 1990; Gu and Gillespie, 1998; Kimes and Kirchner, 1981; Saraf, 1998).

- Biophysical properties of land cover classes which include the landscape spatial structure and ecological factors (Dozier and Frew, 1990; Ekstrand, 1996).

Unfortunately, radiation transfer models are not widely available to the scientific community to sort out this environmental complexity, and scientists must use simplistic procedures and satellite data to extract environmental information. It is notoriously difficult to determine if spectral variation in satellite imagery is representative of real biophysical characteristics, given all the environmental factors influencing reflectance. Consequently, anisotropic-reflectance correction of satellite data is required before environmental information extraction procedures can be implemented (Hugli and Frei, 1983; Meyer et al., 1993).

Numerous investigators have attempted anisotropic-reflectance correction to account for atmospheric and topographic effects using empirical approaches and physical models (Bishop et al., 1998a; Colby, 1991; Gu and Gillespie, 1998; Kimes and Kirchner, 1981; Meyer et al., 1993; Smith et al., 1980, e.g.). In mountain environments, topography represents the most significant source of spectral variation (Duguay and LeDrew, 1992; Gu and Gillespie, 1998; Hugli and Frei, 1983; Kimes and Kirchner, 1981; Teillet et al., 1982), as topographic complexity can produce low, moderate, and high frequency spectral variation in satellite imagery. The term *anisotropic-reflectance correction* refers to radiometric calibration procedures that reduce spectral variation in satellite imagery caused by topography

and other factors (Colby, 1991; Conese et al., 1993a; Civco, 1989; Gu and Gillespie, 1998; Ekstrand, 1996). Many earth scientists use the term *topographic normalization*, although the term anisotropic-reflectance correction is technically more accurate.

1.1 Nature of the Problem

The problem of anisotropic reflectance is a significant one in the field of remote sensing science (Colby, 1991; Bishop et al., 1998a; Hugli and Frei, 1983). The topography plays a critical role, as radiation interacts with the atmosphere and topography, such that all irradiance components are partly controlled by the topographic characteristics of an area. For example, altitude variations within an area alter the atmospheric optical depth (τ_a), such that atmospheric attenuation of the direct irradiance varies as a function of the local relief. Consequently, the magnitude of the direct irradiance at the surface (E_λ^b), must be less than the exoatmospheric irradiance (E_λ^0), because of the aforementioned factors and local topography (i.e. slope and slope aspect).

The topography also influences the magnitude of the diffuse skylight irradiance (E_λ^d), as it shields portions of the landscape from irradiance caused from atmospheric scattering. Furthermore, the nature of the topography determines the magnitude of the adjacent-terrain irradiance (E_λ^T), which varies as a function of local terrain parameters and land cover characteristics. Collectively, mountain topography largely dictates the magnitude of spectral irradiance that reaches the earth surface. Variation in spectral irradiance is generally referred to as *differential illumination*, and causes shadows to be present in satellite imagery.

Anisotropic-reflectance correction attempts to reduce spectral variation in satellite imagery caused from the irradiant and radiant flux.

Numerous investigators have attempted to normalilze satellite imagery in a variety of mountain environments with limited degrees of success (Civco, 1989; Colby, 1991; Conese et al., 1993a; Ekstrand, 1996; Gu and Gillespie, 1998). The results can be attributed to different environments and methodological procedures. Specific approaches that have been investigated include:

1. Use of spectral features such as image ratios and principal components (Colby, 1991; Conese et al., 1993a; Yool et al., 1986).

2. Use of empirical equations to address site specific problems (Duguay and LeDrew, 1992; Hugli and Frei, 1983; Meyer et al., 1993).

3. The use of the Lambertian assumption and the Cosine correction (Richter, 1997; Civco, 1989; Hugli and Frei, 1983; Meyer et al., 1993; Smith et al., 1980).

4. The use of the non-Lambertian assumption and the Minnaert correction (Bishop et al., 1998b; Ekstrand, 1996; Meyer et al., 1993; Colby, 1991; Teillet et al., 1982)

5. The development and testing of new classification algorithms (Meyer et al., 1993; Yool et al., 1986).

6. The use of physical models (i.e., radiative transfer models, LOTRAN, MOTRAN) (Greuell and de Wildt, 1999; Meyer et al., 1993).

Results indicate that there is a need to re-evaluate empirical approaches, as they have been found not to be universally applicable. Furthermore, many approaches have not been thoroughly evaluated in a quantitative fashion, addressing the issue of scale-dependent spectral variation.

Numerous studies have attempted to use the Cosine-correction method to reduce spectral variation. Research indicates that the Lambertian assumption is not effective for anisotropic-reflectance correction in areas of complex mountainous terrain (Colby, 1991; Meyer et al., 1993). Consequently, researchers have investigated other procedures that may have the potential to be used on an operational basis (Bishop et al., 1998a; Ekstrand, 1996; Colby, 1991). Bishop et al. (1998a) indicated that anisotropic reflectance must be thoroughly addressed in high mountain environments, and that topographic normalization procedures have not been thoroughly evaluated. In addition, they indicated that the Minnaert-correction procedure has the potential for further development to address theoretical and operational problems. Therefore, research related to the development and the testing of new procedures and models is warranted. This research focuses on the testing of new implementations of models to support operational assessment and monitoring of the Earth's surface from space.

1.2 Research Objectives

The ultimate objective of this research is to evaluate the utility of the Cosine and Minnaert-correction procedures for anisotropic-reflectance correction of satellite imagery. This re-

search was conducted using SPOT multispectral imagery acquired from Nanga Parbat mountain in Northern Pakistan. The complex topography and extreme relief at Nanga Parbat enabled a thorough assessment of the utility of both procedures for anisotropic-reflectance correction. Specific objectives include:

- Evaluate the utility of the Cosine correction method to normalize SPOT multispectral imagery. Numerous studies have evaluated the Lambertian-reflectance assumption (Richter, 1997; Civco, 1989), and results indicate that the approach can be effectively utilized to reduce spectral variation within a certain range of topographic conditions. The Cosine-correction method has not been evaluated in high mountain environments.

- Evaluate the utility of the Minnaert correction procedure to normalize SPOT multispectral imagery. The model is based upon the use of a Minnaert constant. Global Minnaert constants were to be used to characterize the degree of anistropy. This approach has been used in a variety of mountain environments including the Himalaya (Bishop et al., 1998b; Colby, 1991; Ekstrand, 1996). The objective is to determine if a global Minnaert constant can accurately characterize anisotropic reflectance, given the complex land cover and topographic characteristics at Nanga Parbat.

- Develop and test two new implementations of the Minnaert correction procedure using local and land-cover stratification procedures for calculating multiple Minnaert constants. The new implementations of the model enable multiple Minnaert constants to be used to more accurately characterize anisotropic reflectance caused by

topography and local biophysical properties of the surface.

- Compare modeling results to determine which approach best characterizes anisotropic reflectance and reduces spectral variation in satellite imagery.

1.3 Hypothesis and Rationale

The aforementioned objectives highlight the need to verify various aspects of radiative transfer theory and model existing ideas that have not been thoroughly tested. Given the complexity of radiation transfer theory, it is appropriate to simplify the mathematical characterization of fundamental components, which dictate the magnitude of reflectance recorded by the sensor system. Figure 1 is a simplification of the theory which is the basis of this research.

- The Lambertian assumption and use of the Cosine-correction method works well for surfaces that exhibit isotropic reflectance (Hugli and Frei, 1983; Jin and Simpson, 1999). When studying mountain environments, one can make the assumption of isotropic reflectance, although research indicates that this assumption is invalid in rugged terrain (Hugli and Frei, 1983). Consequently, it was hypothesized that the Cosine correction method would not work at Nanga Parbat, or in other complex mountain environments.

  This hypothesis is based upon the fundamentals of radiation-transfer theory which dictates that steep slopes and land cover should produce anisotropic reflectance. The

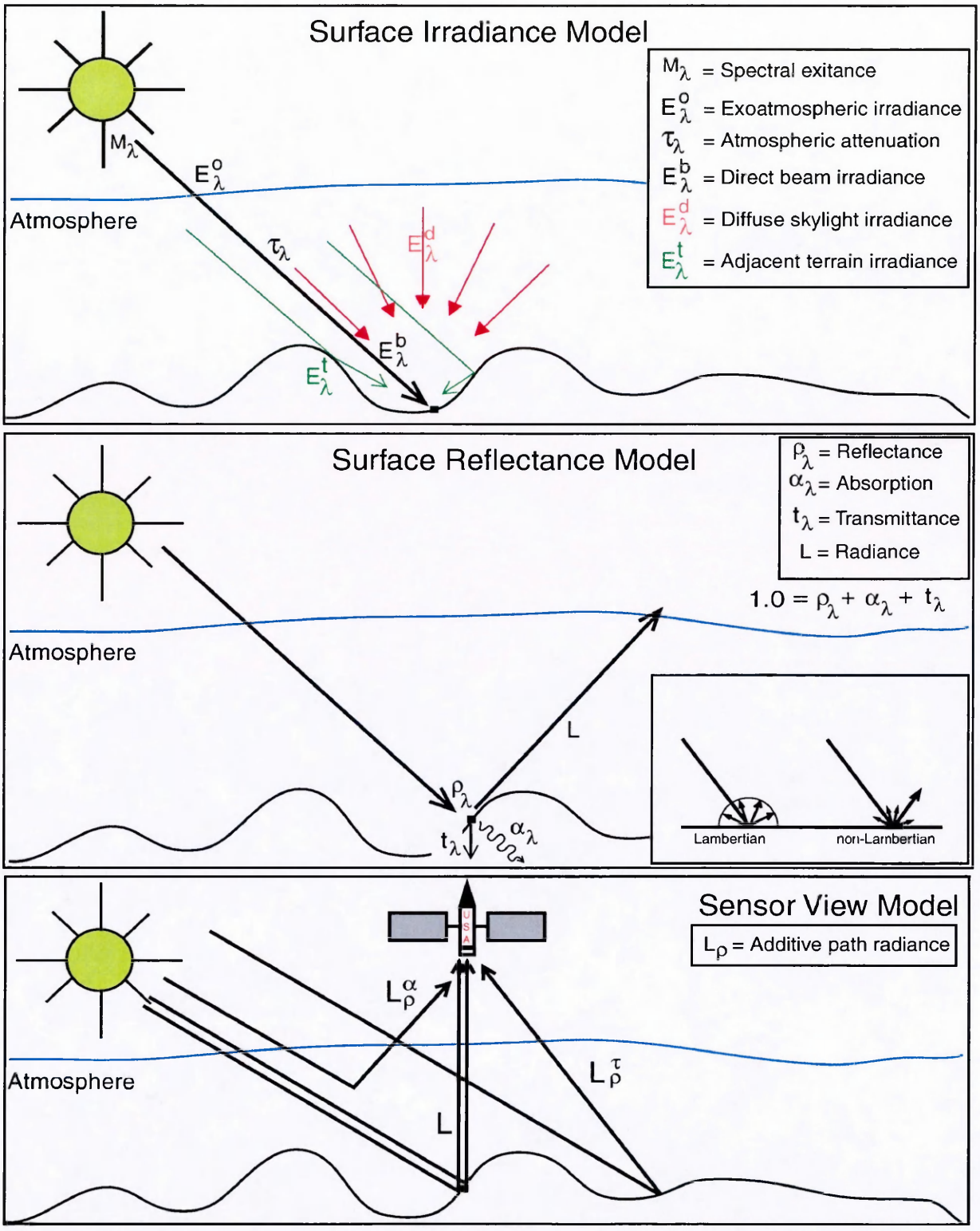

Figure 1: Conceptual model of radiative transfer components for passive remote sensing of the environment. Upper diagram represents the irradiance submodel. Middle diagram represents matter/energy interactions and reflectance models. Lower diagram represents the sensor viewing components.

Lambertian assumption represents isotropic reflectance and this assumption is accounted for by utilizing the magnitude of the direct irradiance, which only takes local topographic conditions into consideration. Because the Cosine correction procedure utilizes a proxy for this irradiance component ($cosi$), we might expect that in areas with steep slopes, the modeled irradiance proxy will be significantly underestimated. This would result in the over-correction of satellite imagery in areas of complex topography. We might however, expect the model to do a reasonable job in areas with low slope angles and homogeneous land cover (Civco, 1989, e.g.). Nanga Parbat, however, exhibits extreme relief. Therefore, the Cosine-correction procedure is unlikely to be useful for anisotropic-reflectance correction.

- The Minnaert-correction procedure makes the assumption that the surface can exhibit isotropic or anisotropic reflectance (Hugli and Frei, 1983). Mathematically, this can be represented by the Minnaert constant which attempts to characterize reflectance (i.e., a Minnaert constant in which $k = 1.0$ would indicate isotropic reflectance and $k < 1$ would indicate anisotropic reflectance). In addition, the Minnaert-correction procedure includes a proxy for the direct irradiance and the viewing exitance angle in order to calculate k. Consequently, it is hypothesized that the Minnaert-correction procedure is more robust and has the potential to be used for anisotropic-reflectance correction. It was hypothesized that the use of global Minnaert constants, however, would not accurately characterize anisotropic reflectance caused by land cover. It was expected that normalized imagery will visually appear to be superior to the Cosine

correction method.

This hypothesis is based upon the idea that one Minnaert constant cannot accurately characterize anisotropic reflectance within an area that is heterogeneous with respect to topography and land cover. The procedure requires a numerical solution where spectral and topographic variability must be accurately modeled to account for linear variation. This is virtually impossible to achieve with one Minnaert constant. Application of the model forces a linear solution, which will result in valid anisotropic-reflectance correction for a relatively low percentage of pixels.

- Image-segmentation approaches will enable the generation of multiple Minnaert constants to be used to characterize anisotropic reflectance throughout the scene. By using a sliding-window approach, one can simplistically account for land cover and topographic variations. In fact, Colby (1991) stated that local Minnaert constants should produce better results. Image segmentation based upon land cover patterns, should also be useful as land cover and biophysical variations can be used to stratify the image and produce multiple Minnaert constants based upon the spatial complexity of the landscape. In theory, both implementations should produce a reasonable solution. In practice, it is hypothesized that the local-window approach will not work very well, unless a dynamic procedure is used that automatically accounts for topographic and land-cover variation. Furthermore, it is hypothesized that the land-cover stratification approach will produce Minnaert constants that accurately characterize the degree of anisotropy. Therefore, it is theorized that in order to effectively nor-

malize satellite imagery in complex mountainous terrain, a spatial analysis of spectral and topographic information must be used.

The aforementioned hypotheses are based upon the knowledge that land-surface biophysical properties partially dictate the bi-directional, reflectance-distribution fraction (BRDF). Consequently, we might expect the window-stratification approach to work well if homogeneous land cover characteristics are present. One would need to know the scale-dependent characteristics of topography and land cover to select an appropriate window size. In the Himalaya, knowledge of scale-dependent characteristics of these properties are largely unknown (Shroder and Bishop, 1998). Therefore, small window sizes should reasonably account for land cover, but not sample enough topographic variation to account for anisotropic reflectance caused by topography. Conversely, large window sizes should capture topographic variability, but sample multiple land-cover classes. Theoretically, the approach is limited by the need for *a priori* knowledge and an understanding of process dynamics which define the scale-dependent spatial structure of the landscape.

The land-cover stratification approach addresses the specific limitations of the sliding-window approach. Land-cover classes define the number of Minnaert constants that will be used. Theoretically, this should produce superior results and enable operational topographic normalization because the approach samples topographic variation within the spatial extent of a land cover class.

- The ultimate objective of this work is to determine which of the aforementioned pro-

cedures will effectively reduce spectral variation in images caused by topography. Although a variety of investigators have evaluated topographic-normalization procedures in mountain environments, they have not thoroughly evaluated these models from a geostatistical perspective (Bishop and Colby, 2002). If a dynamic-landscape analysis procedure can account for spectral and topographic variation, then it is hypothesized that image normalization will result in relatively high spectral variation. This hypothesis must be qualified so that it does not include variance that is the result of a lower signal-to-noise ratio. In addition, higher spectral variance must be associated with valid Minnaert constants, as defined by regression analysis and statistically significant r^2 values.

1.4 Definition of Terms

This research is based upon radiation transfer theory. Radiation parameters are formally defined to operationally define the research problem.

- *Exoatmospheric spectral irradiance* - This term refers to the incoming direct solar irradiance at the top of the atmosphere (E^0_λ, [W $m^{-2}sr^{-1}\mu m^{-1}$]). The magnitude of this parameter is dependent upon the spectral exitance of the Sun (M_λ) and the distance between the Earth and the Sun given the date of image acquisition.

- *Atmospheric attenuation* - This term is used to collectively refer to processes that reduce the magnitude of direct solar irradiance, as it propagates through the Earth's atmosphere. This process can be characterized by an atmospheric-attenuation coef-

ficient (τ_λ^a), which takes into consideration atmospheric scattering, absorption, and refraction by the different components of the atmosphere. This parameter can be estimated using atmospheric-transmission coefficients for specific constituents of the atmosphere such that:

$$\tau_\lambda^a = \tau_\lambda^r \tau_\lambda^m \tau_\lambda^{H_2O}, \tag{1}$$

where τ_λ^r represents attenuation due to Rayleigh scattering, τ_λ^m is attenuation due to Mie scattering, and $\tau_\lambda^{H_2O}$ represents attenuation due to absorption from water vapor.

- *Direct/Beam irradiance* - This term refers to the magnitude of direct solar irradiance reaching the Earth's surface (E_λ^b, [W $m^{-2}sr^{-1}\mu$ m^{-1}]). Because the atmosphere and topography modifies the magnitude of the direct component, it is defined as:

$$E_\lambda^b = E_\lambda^0 \tau_\lambda^a \cos i. \tag{2}$$

where i is the incidence angle, and $\cos i$ represents a modification coefficient that accounts for the Sun-illumination geometry and local topography. It is defined as:

$$\cos i = \cos\theta_s \cos\beta_T + \sin\theta_s \sin\beta_T \cos(\phi_T - \phi_s), \tag{3}$$

where θ_s is the solar zenith angle, β_T is the slope angle of the terrain, ϕ_s is the solar-azimuth angle, and ϕ_T is the slope-aspect angle of the terrain.

- *Diffuse-skylight irradiance* - This term refers to the hemispherical diffuse skylight irradiance that is the result of atmospheric scattering (E_λ^d, $[Wm^{-2}sr^{-1}\mu m^{-1}]$). This component is affected by the topography that shields a portion of the atmosphere.

Topographic shielding is dependent upon topographic complexity and the magnitude of local relief.

- *Adjacent-terrain irradiance* - This term refers to the irradiance incident on a surface resulting from surface reflectance of the adjacent terrain (E_λ^T, $[Wm^{-2}sr^{-1}\mu m^{-1}]$). This component is dependent upon terrain characteristics, and land cover.

- *Spectral irradiance* - Spectral irradiance refers to the total irradiance that reaches the surface of the Earth (E_λ, $[Wm^{-2}sr^{-1}\mu m^{-1}]$). It is defined as:

$$E_\lambda = E_\lambda^b + E_\lambda^d + E_\lambda^T. \tag{4}$$

- *Surface reflectance* - This term refers to a reflectance coefficient (ρ) which is based upon the conservation of energy. It is defined as the fraction of energy reflected from a landscape feature, given the total irradiance (E_λ), such that:

$$1.0 = \rho_\lambda + \alpha_\lambda + t_\lambda, \tag{5}$$

where, α_λ is an absorption coefficient, and t_λ is an attenuation coefficient. It is important to note that when $t_\lambda = 0.0, \alpha_\lambda$ is equivalent to the emissivity of the object (ε_λ).

- *Spectral radiance* - Spectral radiance (L_λ, $[Wm^{-2}sr^{-1}\mu m^{-1}]$) is the radiant flux per solid angle leaving an extended source in a given direction.

- *Lambertian Reflectance* - For most remote sensing studies, it is assumed that the magnitude of radiance is equal in all directions (i.e. isotropic). This simplification is

referred to as the *Lambertian assumption* or *Lambertian model.* For imagery, it can mathematically be defined as follows:

$$L_{xy\lambda} = \rho_\lambda \left[\frac{E_\lambda}{\pi}\right], \tag{6}$$

where x and y refer to image pixel coordinates.

- *Non-Lambertian Reflectance* - Non-Lambertian reflectance refers to anisotropic reflectance, such that the magnitude of reflectance varies as a function of topography and land cover. This can be mathematically characterized in numerous ways, although in this study, a non-linear approach will be used to characterize the magnitude of radiance recorded by the sensor. The Minnaert model is defined as follows:

$$L_\lambda = L_n \cos^{k_\lambda} i \cos^{k_\lambda - 1} e \tag{7}$$

where e is the exitance angle and k_λ is the Minnaert constant which characterizes the departure from isotropic reflectance.

- *Additive path radiance* - This term refers to the radiance that is recorded by a sensor which is not the result of reflectance from the target. The additive path radiance term (L_ρ) is the result of atmospheric effects (L_ρ^a) and adjacent terrain affects (L_ρ^T), such that:

$$L_\rho = L_\rho^a + L_\rho^T. \tag{8}$$

1.5 Significance of Research

World governments are struggling to deal with the issues of population growth, resource allocation, and global environmental change. It has become clear that we will not be able to address these difficult issues without a better understanding of Earth's complex systems. This requires an understanding of process dynamics at the appropriate spatial and temporal scales. Furthermore, it requires operational assessment and monitoring from space.

Currently, the scientific community does not have an operational model to address the difficult problem of anisotropic reflectance. With the advent of new hyper-spectral sensor systems, scientists will have the opportunity to extract new information from satellite imagery that can be used for decision making and problem solving. In mountain environments, this information is critical as hazards, deforestation, and other resource issues are dramatically affecting large populations. The idea of sustainable communities in mountain environments requires basic information and planning. Satellite imagery that has not been corrected for anisotropic reflectance will introduce error into analysis and modeling of the environment. Therefore, scientists must create models that accurately characterize anisotropic reflectance. This modeling is also required to estimate radiation parameters that control processes in climatology, glaciology, geomorphology and ecology, which are all important when trying to model changing earth processes, especially that of global warming.

2 Literature Review

With existing satellite data and a new generation of earth-observing sensors in orbit, earth scientists have access to spatial and temporal data that can provide insights into scale-dependent processes, environmental change, and earth-system dynamics (Davis et al., 1991; Goward and Williams, 1997). Similarly, resource managers and planners can use satellite data to assess and monitor resources and address resource-related issues. Given the advent of geographic information system (GIS) technology, Earth scientists are increasingly dependent on satellite imagery and digital elevation models (DEMs) (Price and Heywood, 1994).

The availability of new data and technology, however, does not directly translate to accurate land-surface characterization and thematic mapping, as information extraction from satellite imagery and spatial data sets is a complex problem. Although a few biophysical properties of the landscape can be directly estimated from remotely sensed data (i.e., altitude, reflectance, albedo, temperature), information extraction requires an understanding of radiation transfer processes (Proy et al., 1989; Chavez, 1996).

Perhaps the biggest obstacle to information extraction in rugged terrain is the problem of anisotropic reflectance. Numerous environmental factors such as the atmosphere, topography, and land cover, dictate the irradiant and radiant flux. Other factors such as solar and sensor geometry must also be taken into consideration, such that the magnitude of the radiant flux varies in all directions (anisotropic reflectance). Consequently, anisotropic-reflectance correction of satellite imagery is required so that image radiance variations cor-

respond to variations in the biophysical characteristics of the landscape (Smith et al., 1980; Chavez, 1996). Attempting to do this in rugged terrain, is very difficult, as topographic effects influence radiation transfer at a variety of scales (Hugli and Frei, 1983; Yang and Vidal, 1990; Gu and Gillespie, 1998).

Earth scientists working with satellite imagery in rugged terrain, must correct for the influence of topography on spectral response (Smith et al., 1980; Proy et al., 1989; Bishop and Colby, 2002). The literature refers to this as the removal or reduction of the *topographic effect* in satellite imagery, and it is generally referred to as *topographic normalization* (e.g., Civco, 1989; Colby, 1991; Conese et al., 1993b; Gu and Gillespie, 1998).

The nature of the problem, however, is extremely complex, as at-satellite radiance is governed by scale-dependent radiative transfer interactions between atmosphere, topography, and land cover characteristics (Kimes and Kirchner, 1981; Proy et al., 1989; Yang and Vidal, 1990). From a physical-modeling perspective, the problem is one of anisotropic-reflectance correction (ARC), as various environmental factors dictate the irradiant flux and the bi-directional reflectance distribution function (BRDF). From an applications point of view, ARC is required to accurately map natural resources and estimate important land-surface parameters (Yang and Vidal, 1990; Colby and Keating, 1998).

Research into this problem has been ongoing for about twenty years. To date, an effective ARC model to study anisotropic reflectance in mountain environments has yet to materialize. Gemmel (1998) suggested the coupling of an atmospheric model with a BRDF model and a DEM. Much research has focused on radiative transfer modeling and the use of

the Lambertian assumption for simplification purposes. This assumption, however, is not appropriate in rugged terrain, and scale-dependent, topographic effects must be considered (Proy et al., 1989; Giles, 2001; Bishop and Colby, 2002).

Various approaches have been used to reduce spectral variability caused by the topography. They include: 1) Spectral-feature extraction. Various techniques are applied to satellite images and new spectral-feature images are used for subsequent analysis; 2) Semi-empirical modeling. The influence of the topography on spectral response is modeled by using a DEM; 3) Empirical modeling. Empirical equations are developed by characterizing scene-dependent relationships between reflectance and topography, and; 4) Physical models. Various components of the radiative transfer process are modeled.

The different approaches have their advantages and disadvantages with respect to computation, radiometric accuracy and application suitability. Spectral-feature extraction and the use of spectral ratios and principal-components analysis (PCA) has been used by a variety of investigators (Conese et al., 1993b; Ekstrand, 1996). Research indicates that ratioing and PCA can be used, although several issues must be considered.

For example, spectral-band ratioing has been used to reduce the topographic effect (Kowalik et al., 1983; Ekstrand, 1996). It is important, however, to account for atmospheric effects such as the additive path-radiance term before ratioing (Kowalik et al., 1983). This dictates that DN values must be converted to radiance and atmospheric-correction procedures accurately account for optical-depth variations. The altitude-atmosphere interactions are almost never considered, and information may be lost in areas where cast shadows are

present. One might also expect that ratioing using visible bands may not be effective due to the influence of the atmosphere at these wavelengths. Ekstrand (1996) found this to be the case and indicated that the blue and green regions of the spectrum should not be used for ratioing to reduce the topographic effect. Furthermore, for biophysical remote sensing, ratioing and PCA do not address the problem, as land-surface estimates cannot be derived from transformed values.

Other investigators have attempted to correct for the influence of topography by accounting for the nature of surface reflectance (Lambertian or non-Lambertian) and the local topographic conditions (Colby, 1991; Ekstrand, 1996; Colby and Keating, 1998). Semi-empirical approaches include Cosine correction (Smith et al., 1980), Minnaert correction (Colby, 1991), the c-correction model (Teillet et al., 1982), and other empirical corrections that make use of a DEM to account for the local illumination conditions for each pixel. These models have been widely applied given their relative simplicity and ease of implementation.

Research findings indicate that these approaches may work, only for a given range of topographic conditions (Smith et al., 1980; Richter, 1997), and they have similar problems (Civco, 1989). For example, the Cosine-correction model does not work in rugged terrain. Smith et al. (1980) produced reasonable results for terrain where slope angles and solar-zenith angles were relatively low. Numerous investigators have found that this approach overcorrects and cannot be used in a variety of mountain environments (Civco, 1989; Bishop and Colby, 2002).

The Minnaert-correction procedure has been frequently used, as it assumes non-Lambertian reflectance, and accounts for the view angle of the sensor. It relies on the use of a globally derived Minnaert constant (k), to characterize reflectance and its departure from Lambertian. Ekstrand (1996) found the use of one fixed k value to be inadequate in a study in southwestern Sweden, and other work has suggested that local k values may be needed (Colby, 1991). Overcorrection can still be a problem, and this led Teillet et al. (1982) to propose the c-correction model, where c represents an empirical correction coefficient that lacks any exact physical explanation. Other empirical models, which are based upon the relationship between radiance and the direct solar irradiance, have similar problems and are not usable for some applications (Gu and Gillespie, 1998).

Given the popularity of the Minnaert-correction model, Bishop and Colby (2002) tested it in the western Himalaya and found that the current implementation of the model for large areas has limited utility, because high r^2 values are required for the computation of k, multiple Minnaert coefficients (k is not a true constant) are required to characterize anisotropic reflectance caused by land cover, and the direct irradiance component is inadequate for representing the total irradiant flux. Furthermore, they found that ARC can alter the spatially dependent variance structure of satellite imagery in an incorrect way, even though the topographic effect appears to be removed or reduced.

Most recently, the new ERDAS ATCOR3 model (Erdas, 2001) attempts to integrate a radiative transfer model and a simple BRDF to accomplish ARC. Model simplifications, however, are based upon computational feasibility and inference, rather than a true under-

standing of scale-dependent, topographic effects.

The aforementioned problems are the result of ignoring scale-dependent topographic effects (Proy et al., 1989; Giles, 2001). Previous research has not provided the linkage between radiation transfer and a non-Lambertian representation of surface reflectance at the same time. Furthermore, the degree of anisotropy is wavelength dependent and must be considered (e.g. Greuell and de Wildt, 1999).

The ideal situation is to develop physical models that account for all the radiative transfer interactions at altitude. This is currently not feasible, as accurate estimates for a multitude of parameters are required, and the problem is computationally intractable (Hugli and Frei, 1983; Proy et al., 1989; Yang and Vidal, 1990). Progress has been made, however, in understanding and modeling various atmospheric and topographic effects from point data, such that the significance of the primary irradiance components can be inferred (e.g. Proy et al., 1989).

Given the non-Lambertian nature of snow, ice, forest canopies and other surfaces (Dozier, 1980; Hall et al., 1989; Gu and Gillespie, 1998), more research is required to understand complex scale-dependent, radiation-transfer processes. Furthermore, field research in mountains is required to characterize the nature of the irradiant flux and the BRDF for land-cover classes.

A better understanding will require the development of a spectral solar ARC model that simulates the interaction of radiation with the atmosphere, topography and land cover. A solution dictates finding an acceptable level of simplification to study the scale-dependent,

topographic effects, so that an effective operational ARC model can be developed.

The aforementioned examples illustrate the need to develop and investigate new procedures for anisotropic-reflectance correction. The literature indicates that the Minnaert-correction procedure offers numerous conceptual and implementation advantages if multiple Minnaert constants can be empirically calculated to account for topography and land cover. This research investigates that possibility.

3 Study Area

The study area for this research is the Nanga Parbat massif which is located in northern Pakistan (Figure 2). The majestic peak reaches 8125m high, making Nanga Parbat the 9th largest mountain in the world (Shroder et al., 1999). The landscape is very complex, as the coupling of climate, tectonics, and surface processes has produced a complex mosaic of topograpy and land cover. The landscape exhibits extreme relief, altitudinal gradients, and active geological processes, which are responsible for rapidly changing conditions. From a remote-sensing perspective, this study area represents an extreme environment which is excellent for testing ARC approaches and models. An understanding of this mountain system and its unique landscape characteristics, however, is required in order to effectively evaluate the results of ARC procedures.

3.1 Environmental Setting

Nanga Parbat, due in part to its extreme relief and highly variable terrain, has a wide variety of climatic conditions. The sheer height of the east-west-running mountain ridge acts as a natural divide between the cool, arid air from Asia and the warmer, humid air masses from the Arabian Sea (Shroder et al., 1999). Thus, the northern area of the massif is more arid due to rainshadow effects (Shroder et al., 1999). Peaks within the mountain range can expect average precipitation around 2000 mm $yr^{-}1$. Most of this precipitation comes in the form of snow in the summer, adding to the massive glaciers that reside in the upper reaches of the mountain range (Shroder et al., 1999). The lower valley regions experience less

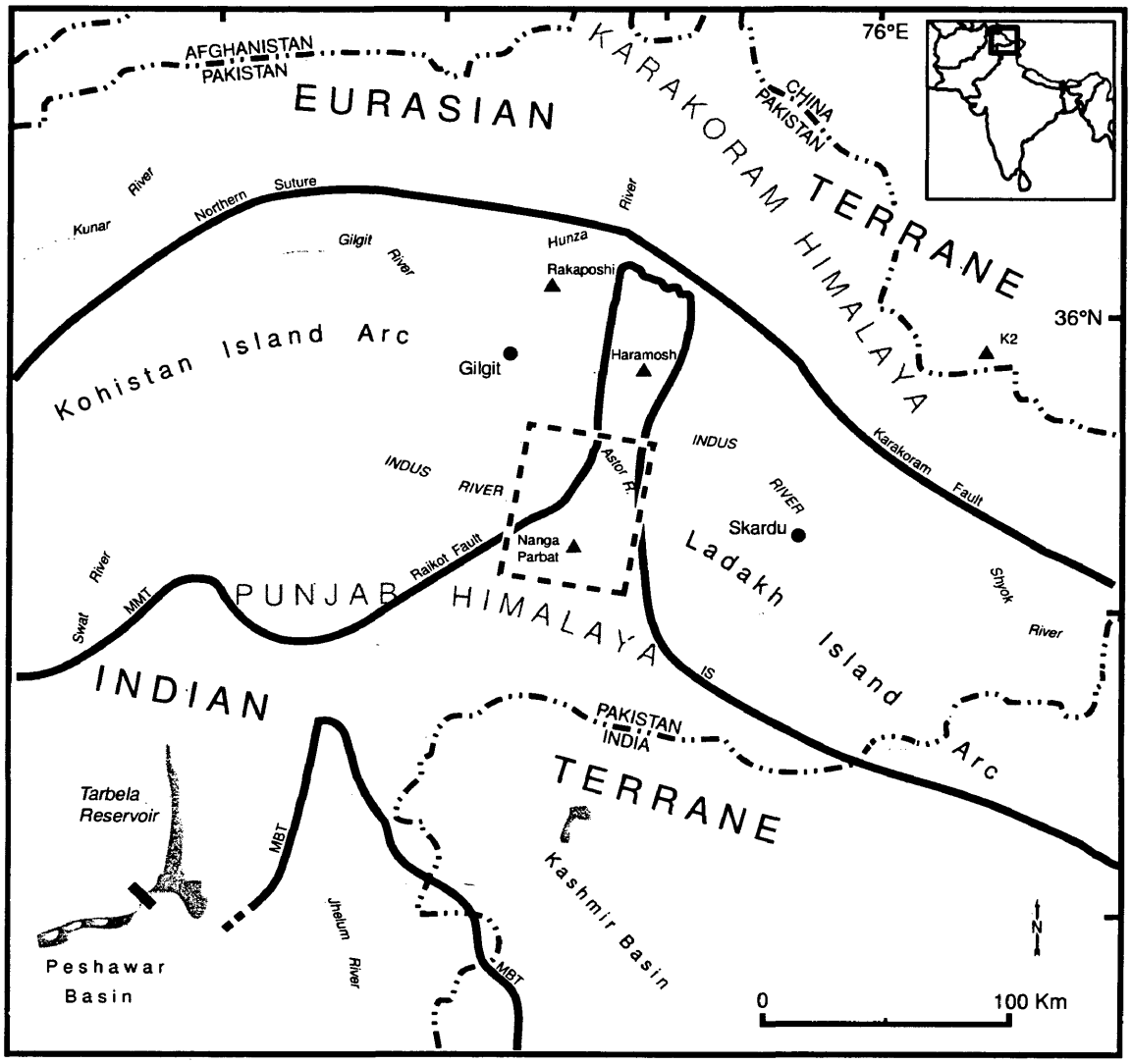

Figure 2: Nanga Parbat in northern Pakistan. Dashed line indicates coverage of SPOT-3 satellite imagery and digital elevation model.

precipitation due to orographic effects. On average, valley areas receive approximately 200 mm of precipitation annually with temperatures reaching 50° C at lower altitudes (Shroder et al., 1999).

The Himalaya is an area of continuing tectonic uplift. Approximately 50 million years ago, the Indian plate began colliding with the Asian plate, and caused crustal uplift (Shroder et al., 1999). Uplift at Nanga Parbat is thought to be caused by rapid denudation (Zeitler et al., 2001) as a kind of focused isostasy. Regional isostatic uplift may also have occurred in the past, but lack of information about the erosion processes over the past $10^4 - 10^3$ Ka, makes it difficult to find supportive evidence (Shroder Jr. and Bishop, 2000). Tectonic activity in this region has also caused extensive faulting throughout the mountain (Shroder et al., 1999).

A variety of surface processes are active at Nanga Parbat and mass movements, river incision and glaciation are the primary agents responsible for erosion and the sediment flux (Shroder Jr. and Bishop, 2000). River incision and slope-failure processes are responsible for the deep "V" shaped valleys at lower altitudes in the Astor, Raikot and Buldar Basins (Figure 3). At intermediate altitudes, debris flows are common as orographic precipitation and monsoon rains transport debris towards the valley bottoms. Shroder et al. (1999) documented the historical and geomorphological evidence for catastrophic flooding in many valleys as a result of glacial blockage of valleys and catastrophic break-out floods caused by subglacial hydrology.

At higher altitudes, the landscape has been dramatically altered by glaciation (Bishop

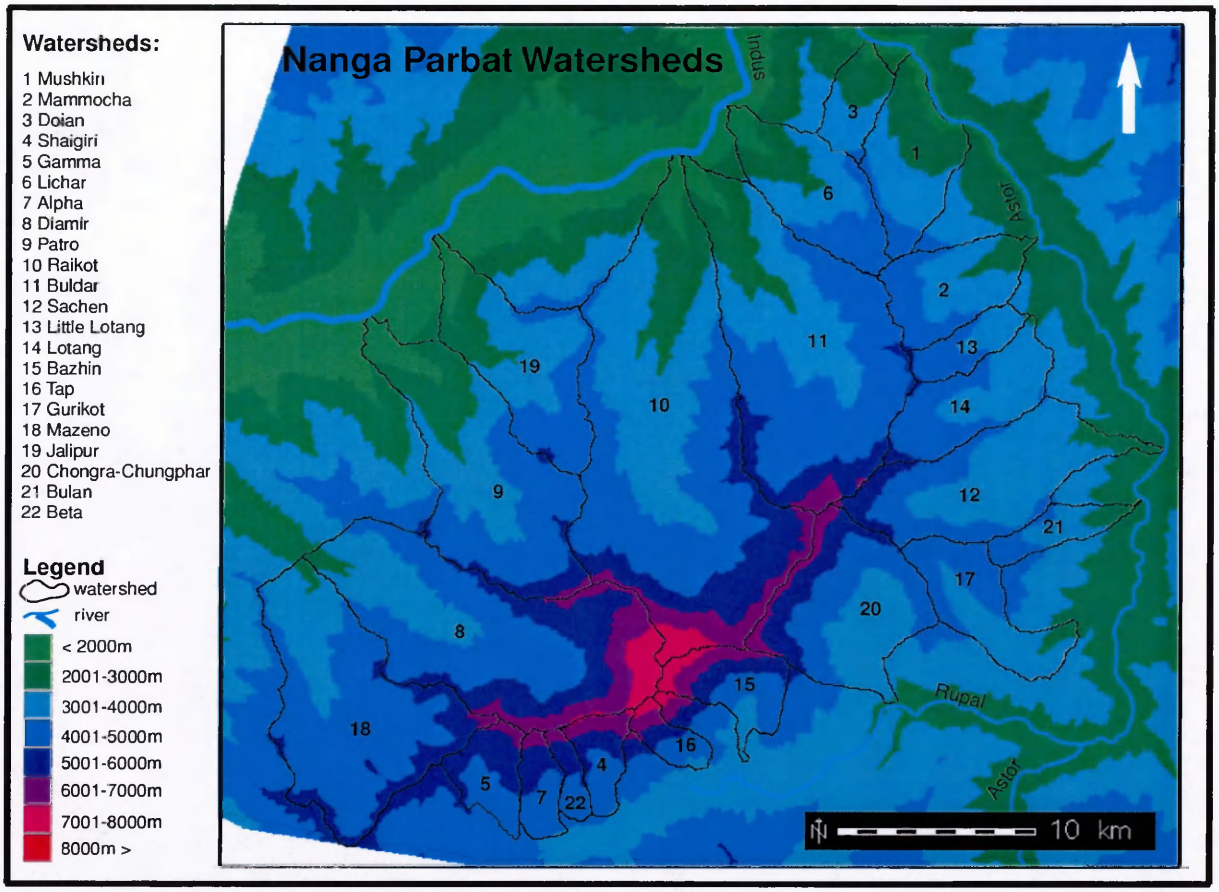

Figure 3: Various watersheds at Nanga Parbat.

and Shroder, 2000; Shroder Jr. and Bishop, 2000). High-altitude erosion surfaces are found in most valleys at an elevation of about 4300 m. These surfaces have been dated by techniques of cosmogenic-exposure age dating, and found to be $\sim$ 65 Ka old. Geomorphological evidence indicates that glaciations in the Holocene also altered the landscape and transported materials out of basins (Phillips et al., 2000; Shroder Jr. and Bishop, 2000). The timing of these glaciations is highly correlated with the southwestern monsoon, and indicates climate forcing played a major role in the topographic evolution of Nanga Parbat. Furthermore, modern-day alpine glaciers are still found all around Nanga Parbat and play

a significant role in the continual denudational unloading of the Nanga Parbat massif.

The extreme relief of Nanga Parbat produces a strong altitudinal climate gradient, which controls the land-cover characteristics. In general, there are five vegetation/land cover classes. At the base of the mountain, 1299 – 2000m, there is a subtropical semi-desert. Vegetation in this area is mostly limited to sage brush. At 2000 – 2900m, a step forest exists. Juniper and pine are the dominant vegetation in this zone. A temperate coniferous forest occurs from 2900 – 3600m, and consists of pine, cedar, spruce and fir. The zone of sub-alpine deciduous forest ranges from 3600 – 5000m. It is composed predominately of birch. Altitudes above 5000m and below the snow line are classified as moist alpine scrub and tundra meadows. Vegetation consists of juniper and grasses, mosses and various shrubs, with the cryosphere extending from the snow line to 8125m. Given the altitudinal zonation of land cover, and tremendous spatial variation in the nature of vegetation, anisotropic reflectance must be accounted for.

The hydrology of the Nanga Parbat region is dynamic and complex. The Indus River, located to the north of the Nanga Parbat massif, is the master stream that is downcutting and eroding the landscape (Figure 3). Burbank et al. (1996) estimated the incision rate, just north of Nanga Parbat, to be $2 - 12$ mm yr^{-1}. The Rupal-Astor river system drains from south to north and is tributary to the Indus. Bishop and Shroder (2000) noted that the Astor River is rapidly incising as it crosses the Raikot Fault where strath terraces document incision of the river into bedrock. Other rivers such as the Raikot, Buldar, and Diamir (Figure 3) radially drain the massif. At lower reaches, they are actively incising in response

to tectonic forcing and this incision produces a distinctive "V" shaped valley.

3.2 Nanga Parbat Topography

Nanga Parbat topography is highly variable in terms of relief and geomorphometric parameters. This is the result of the complex interactions of internal and external forcing factors that control the topographic evolution of the massif. In addition, the overprinting of past surface processes and erosion and deposition further adds to the complexity of the topography. An understanding of the nature of topographic complexity is required, as the topography represents an primary factor controlling the irradiant and radiance flux which affects sensor response.

Numerous investigators have examined the altitude-area distribution of Nanga Parbat and other Himalayan regions using hypsometric analysis (Burbank et al., 1996; Bishop and Shroder, 2000). The hypsometry of Nanga Parbat is presented in (Table 1) and hypsometric curves presented in (Figure 4).

Table 1: Altitude distribution of the landscape at Nanga Parbat.

Altitude (m)	Frequency (%)	Cumulative (%)
1000-1999.9	8.9	8.9
2000-2999.9	18.6	27.5
3000-3999.9	30.8	58.3
4000-4999.9	29.3	87.6
5000-5999.9	8.4	96.0
6000-6999.9	2.9	98.9
7000-7999.9	0.83	99.7
8000-8125.0	0.004	100.0

1995

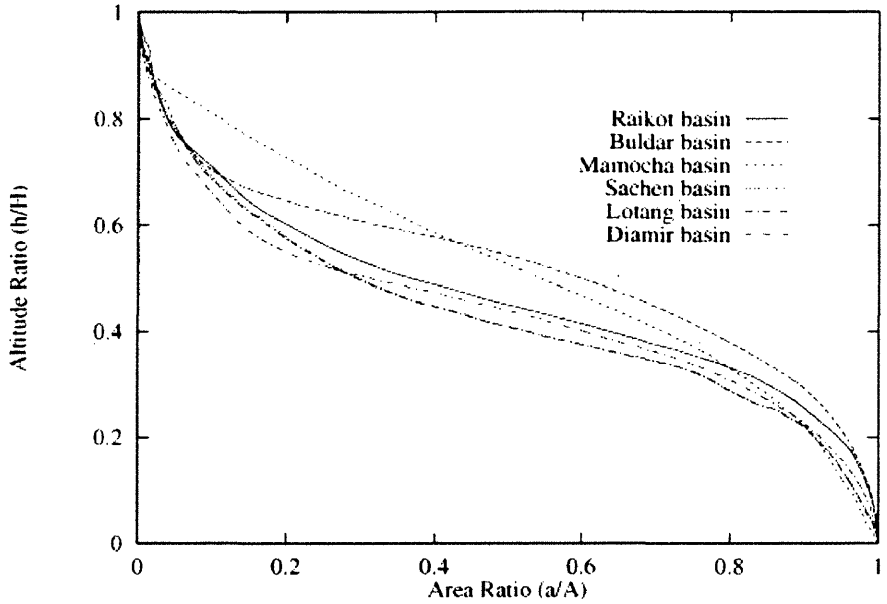

Figure 4: Nanga Parbat basin hypsometry.

The majority of the landscape is at an altitude below 6000 m, while only 4 percent of the landscape represents high altitude. This pattern of altitude represents the interaction of high-magnitude erosion processes and active tectonic uplift which are responsible for the knife-edge ridge and the high altitude of Nanga Parbat (Bishop and Shroder, 2000; Shroder Jr. and Bishop, 2000; Schneider et al., 1999). The regional relief characteristics of the massif are currently controlled by the river incision by the major rivers in the region (Figure 5). Bishop and Shroder (2000) and indicate that the mesoscale relief is highly variable and that glaciation can produce greater relief that river incision at this scale.

The spatial relief characteristics are such that cast shadows can be found in satellite imagery at a variety of scales depending upon the spatial relief structure in relation to the solar geometry. This produces the *topographic effect*, which is present in most imagery obtained over mountains. In general, complex relief patterns increase the spectral variability over

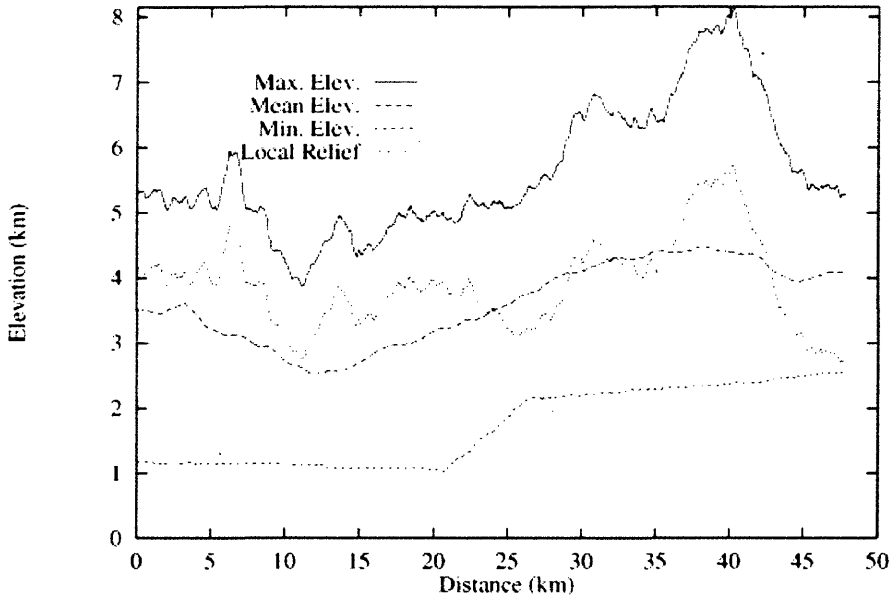

Figure 5: Nanga Parbat swath profiles from North to South.

larger scales and decrease the spectral variability within shadowed areas. These areas can be small, intermediate, or large in size depending upon the spatial complexity of relief.

The mesoscale relief also introduces hemispherical topographic shielding of the diffuse skylight irradiance component (Figure 6). The results show that deep valleys produce concentric shadow patterns that can explain a percentage of the spectral variability in satellite imagery.

Analysis of first-order geomorphometric parameters over Nanga Parbat have been conducted by numerous investigators. Variability in slope angles and slope aspect locally influence the magnitude of the direct irradiance component. Bishop et al. (1998b) conducted slope analysis using a high-resolution DEM. They found that slope angles are highly variable (Figure 7) and that the average slope angle for Nanga Parbat is $\sim 32°$.

Examination of the distribution of slopes indicates that shallow slope angles are as-

Figure 6: Numerical simulation of the hemispherical shielding of the topography on the diffuse irradiant flux. The average shielding coefficient was calculated for a four kilometer radius around each pixel.

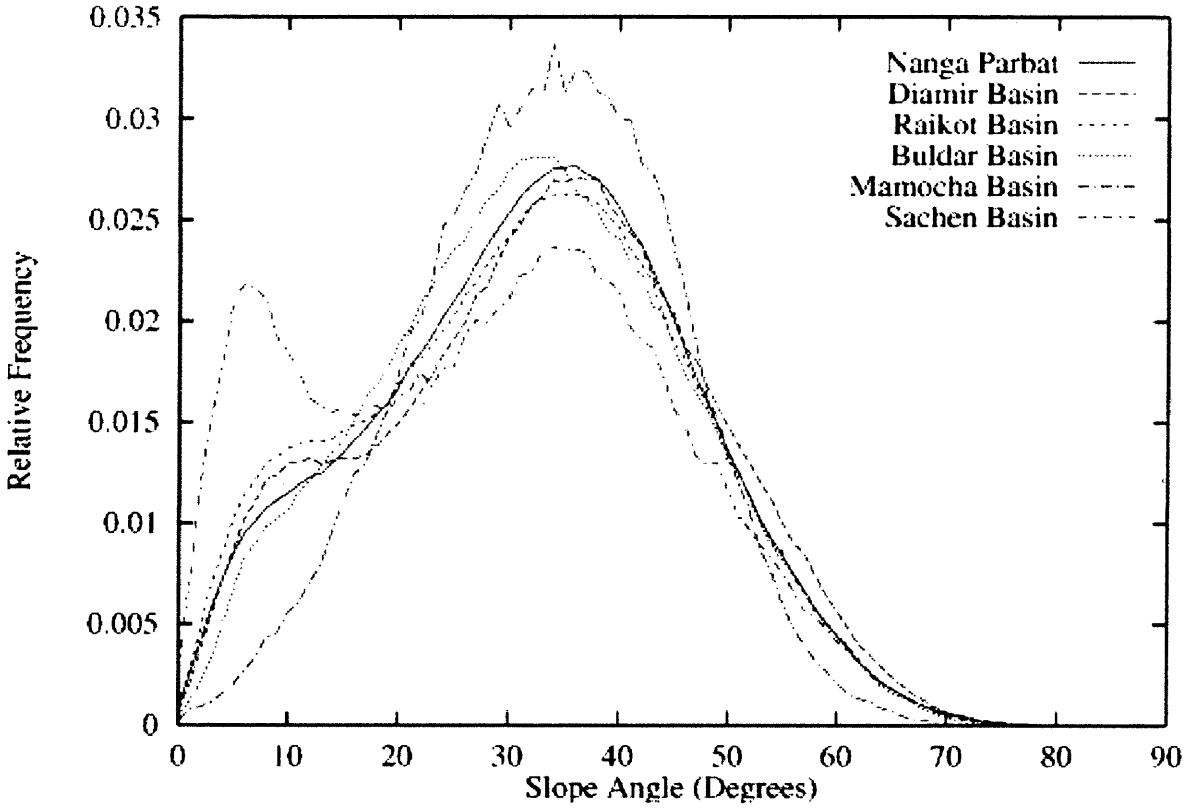

Figure 7: Nanga Parbat slope distributions.

sociated with modern-day glaciation, large landslides, and past glaciations where erosion and/or deposition has modified the landscape, decreasing local relief. Confirmation of this influence of glaciation on the terrain has been verified by several investigators. Specifically, the altitude-slope angle function is not linear (Brozovik et al., 1997; Bishop and Shroder, 2000). Altitude-slope plots clearly reveal steep valley slopes associated with areas of active river incision at lower altitudes (Figure 8).

With increasing altitude, slope angles in valley centers become more shallow, signifying the influence of warm-based glacial erosion and meltwater acting on the topography. With further increasing altitude up to the highest peaks, the magnitude of slope angles increase

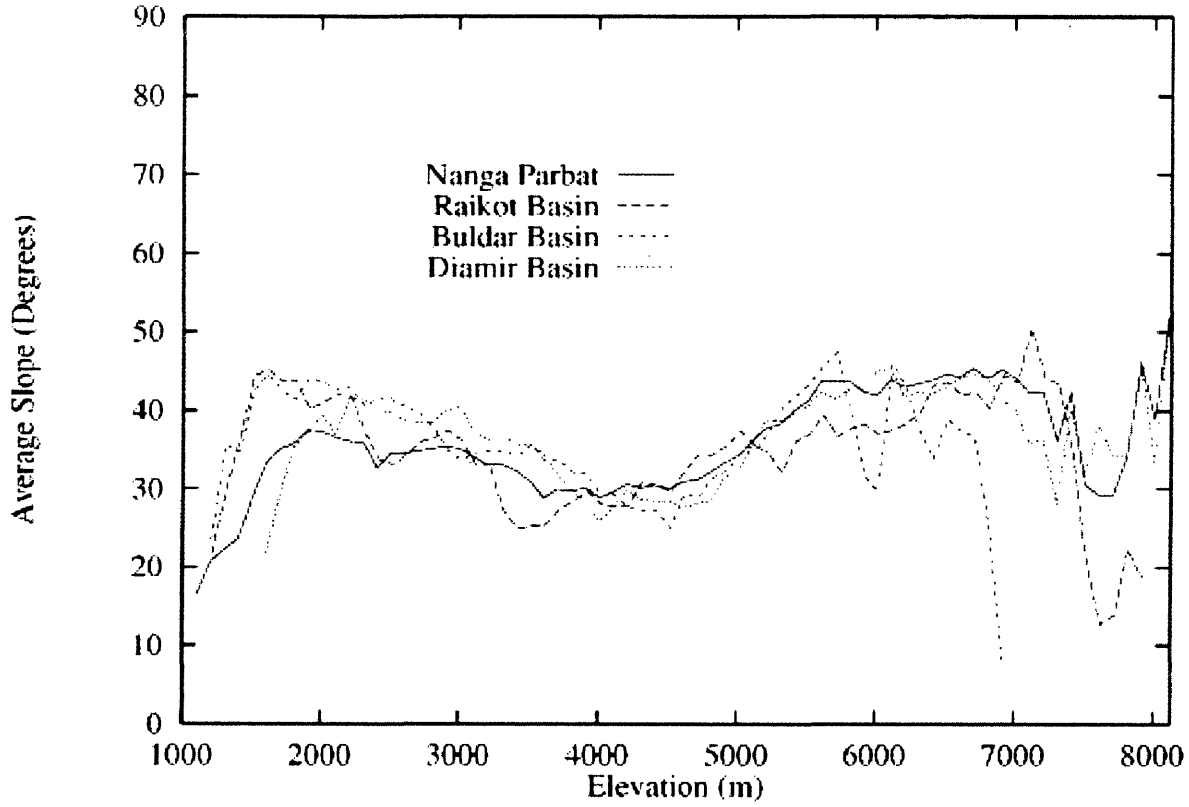

Figure 8: Nanga Parbat slope/altitude relationships.

again, demonstrating the most likely influence of cold-based, protective ice.

The complex spatial patterns of relief, geomorphometric parameters, topographic shielding, and land-cover characteristics, dictate anisotropic reflectance. In theory, the nature of this study area permits the evaluation of numerous factors that significantly influence anisotropic reflectance. An appropriate approach or model should be able to produce spatially consistent results across a range of topographic and land-cover conditions (Bishop and Colby, 2002). Consequently, the Nanga Parbat study area represents an extreme challenge to ARC modeling.

4 Methodology

4.1 Research Design

Anisotropic-reflectance correction of satellite imagery represents a multi-stage processing sequence that attempts to accurately radiometrically calibrate relative spectral-response numbers to units that have physical meaning. This is required for a variety of biophysical applications, as the spatial variance of upward radiance should be caused by biophysical variations of matter on the landscape (i.e. not the atmosphere or topography). A research design was formulated to accomplish the research objectives and test the hypotheses (Figure 9).

The process begins with ortho-rectification of the satellite imagery to correct for the geometric distortion in the imagery caused by the extreme relief at Nanga Parbat. The satellite data were then radiometrically calibrated to account for the sensor gains and biases in recording the upward radiance from the landscape. Various correction procedures were then applied to the satellite imagery to generate new estimates of surface radiance, which in theory, should not be related to the topography.

The modeling phase of the work attempted to determine the validity of various theoretical assumptions associated with radiation transfer in mountain environments. For example, by incorporating land cover into the analysis, it is possible to test the assumption that land cover variations influence the anisotropic nature of reflectance. Similarly, by comparing the Cosine-correction and Minnaert-correction procedures, it was possible to determine what

reflectance model better characterized surface radiance at Nanga Parbat.

A unique statistical evaluation procedure was used to test the results of the Cosine-correction and Minnaert-correction procedures. It is based upon the work of Bishop and Colby (2002) and incorporates the use of descriptive statistics and geostatistics to evaluate the spatial variability in the magnitude of surface radiance after ARC. This is required, as the reduction of the topographic effect in satellite imagery does not mean that the spatial variability in the magnitude of surface radiance is spatially consistent or meaningful (Bishop and Colby, 2002). Consequently, ARC results were rigorously tested, using a variety of traditional and geostatistical approaches. Collectively, the research design enabled the determination of the validity of these ARC procedures and provided insight into the need to develop comprehensive ARC models that integrate additional radiative transfer components which account for the irradiant and radiant flux caused by topography.

4.2 Data Characteristics

The satellite data that were used for ARC was SPOT-3 multispectral imagery. The imagery (Scene ID: 3198279960609055530 1X) was acquired on June 9, 1996 at 5:55:30 GMT. The scene covers an area of 60 km $\times$ 60 km. The sensor generates images in three regions of the electromagnetic spectrum exhibiting a spatial resolution of 20 m. Characteristics of solar geometry for this acquisition date are a solar elevation angle of 71.2° and a solar azimuth of 127.0°. The sensor incident angle was left at 0.9°. The spectral resolution of the data set is as follows:

- SPOT 3 Band 1 (green) $0.50 - 0.59\mu$m.
- SPOT 3 Band 2 (red) $0.61 - 0.68\mu$m.
- SPOT 3 Band 3 (NIR) $0.79 - 0.89\mu$m.

Only the NIR region of the spectrum was used for analysis, as conducting analysis in the visible portion of the spectrum must address numerous issues that are beyond the scope of this study. Examination of the SPOT imagery indicated that the topographic effect was most prevalent in the NIR image (Figure 10).

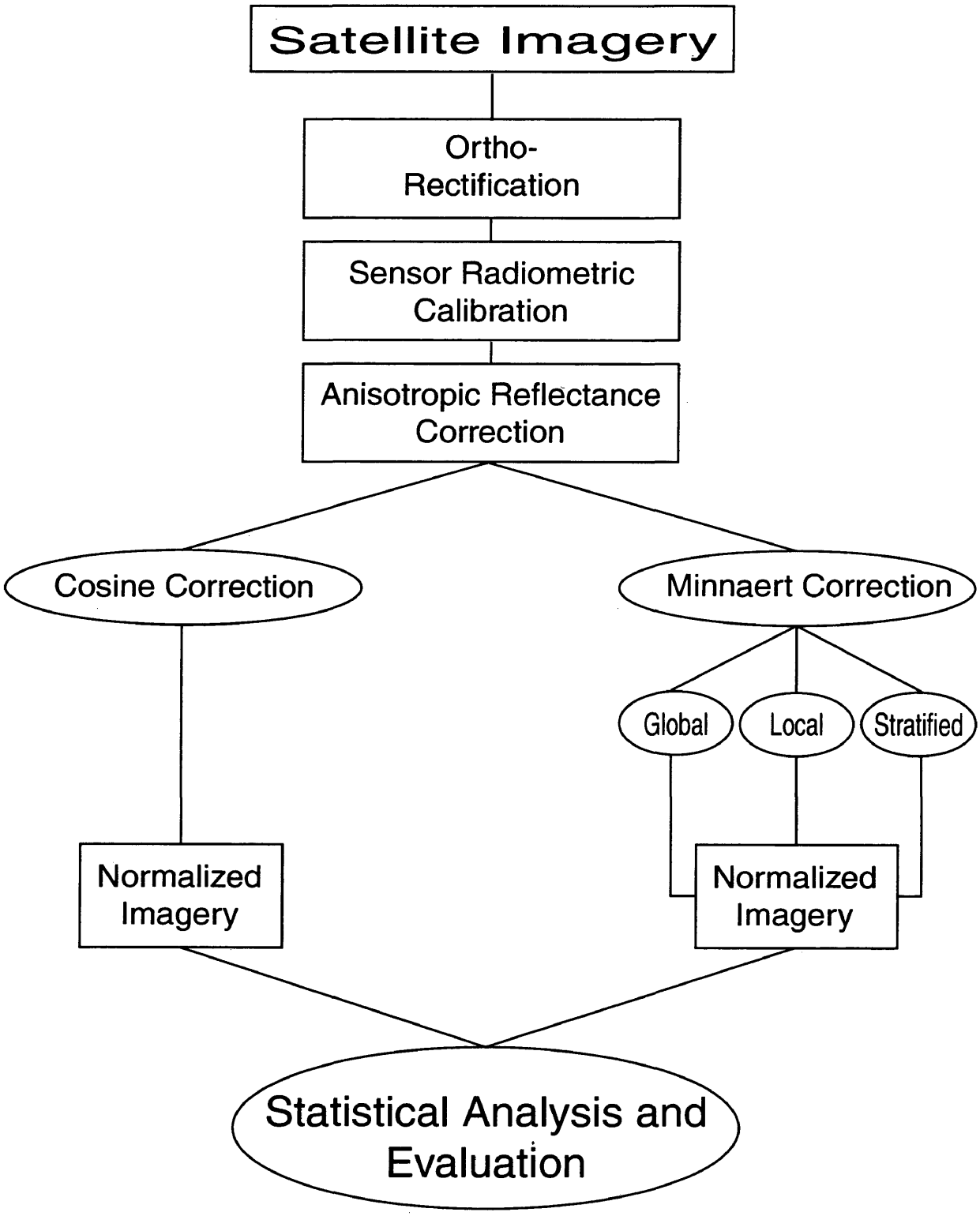

Figure 9: Multi-stage processing sequence design to evaluate anisotropic-reflectance correction procedures.

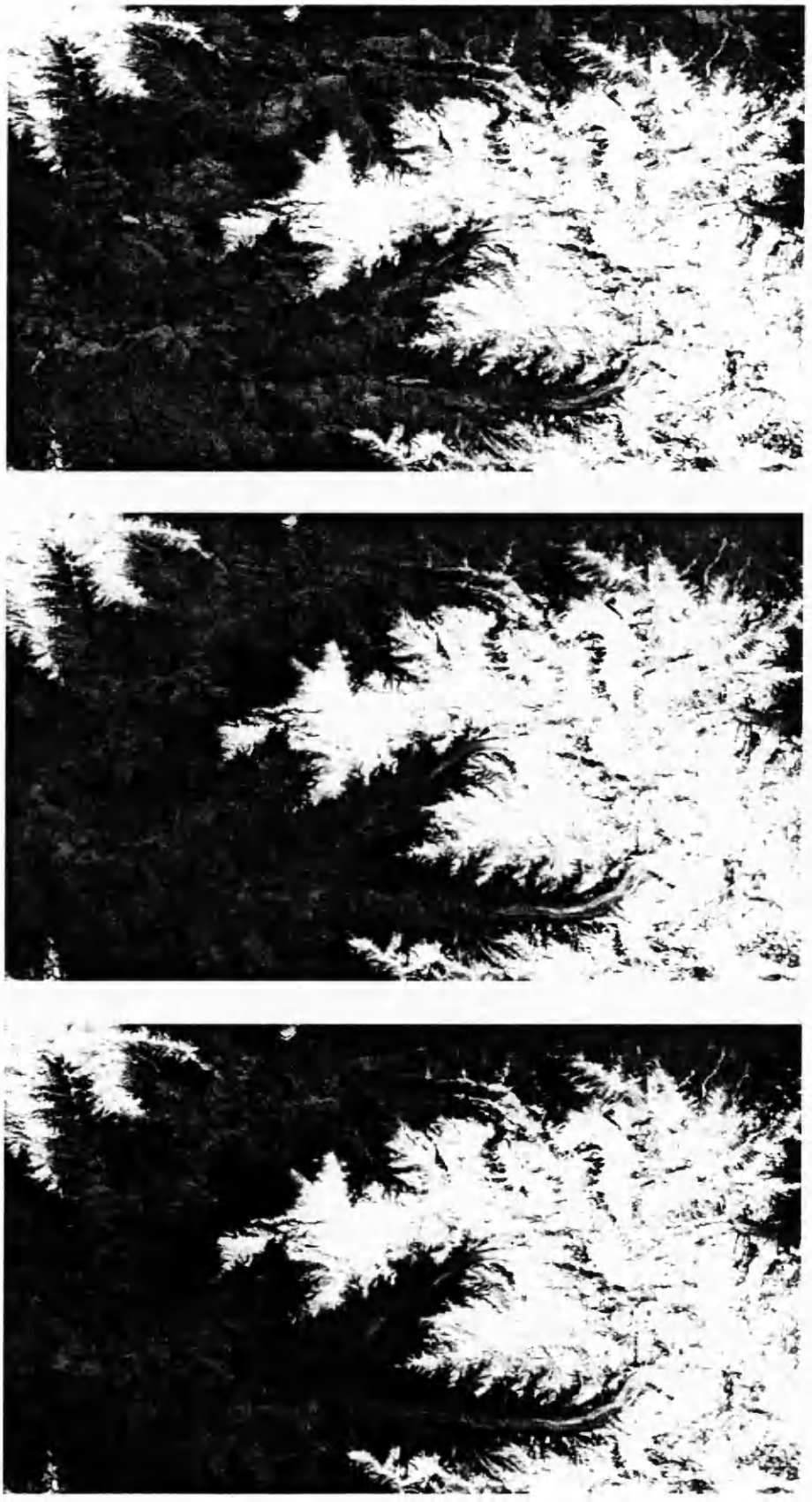

Figure 10: From left to right, SPOT-3 Green, Red and NIR images of Nanga Parbat.

The NIR region of the spectrum is ideal for evaluating ARC procedures, as qualitative visual interpretation can be used to provide a first-order evaluation of ARC results, and the influence of the atmosphere on the irradiant and radiant flux is less than in the visible regions of the spectrum. If the visible spectral bands were used, the influence of the atmosphere must be accounted for and separated from the topographic effects. This is a very complex problem that requires physical atmospheric modeling. It also requires knowing various atmospheric parameters that govern radiation transfer. This is beyond the scope of this research, and in practice, atmospheric conditions are generally not known at the time of image acquisition.

It should also be noted that existing atmospheric correction procedures are in essence, first-order approximations that attempt to correct for the influence of the atmosphere. They assume homogeneous conditions. Atmospheric correction of the NIR image was not applied, as the relief in this area is extreme, and the optical depth of the atmosphere varies significantly over very short distance. Consequently, the atmosphere is not homogeneous and it is not possible to produce a reasonable first-order approximation to account for atmospheric transmissivity and additive path radiance.

Topographic information was required to preprocess satellite imagery and to conduct ARC. SPOT 3 panchromatic stereopairs were obtained to generate a digital elevation model (DEM) of Nanga Parbat (Figure 11). The DEM was used to produce estimates of slope and slope aspect for accounting for variations in the direct irradiant flux caused by topography.

4.3 Image and DEM Preprocessing

The NIR image was co-registered with the DEM in order to conduct analysis. The registration procedure required the use of a DEM, as mountainous terrain generates significant relief displacement and geometric error in imagery (Dozier and Frew, 1990). Consequently, the NIR image was ortho-rectified using Erdas Imagine software so that relief displacement was accounted for and each pixel was assigned real-world coordinates.

This was accomplished using 20 ground control points (GCPs). GCP locations on the landscape were identified in the SPOT imagery and in an ortho-rectified SPOT panchromatic image. A SPOT-3 ortho-rectified panchromatic image was generated by SPOT data corporation using large scale topographic maps. Only static features found in both image data sets were used for rotation and scaling control. The nearest-neighbor interpolation algorithm was used to receive estimates after the rotation. The procedure resulted in a RMSE of less than a pixel (10 m), indicating that the ortho-rectified NIR image was suitable for subsequent analysis (Figure 12).

The ortho-rectified image was then radiometrically calibrated to account for sensor gain and offset biases. This is required as sensor biases can be significant (Chavez, 1996). The relative digital numbers (DN values) were transformed to at-satellite radiance (L, [W m^{-2} $sr^{-1}\mu m^{-1}$]). This was accomplished by utilizing a radiometric calibration coefficient (α_λ) that transforms the DN values into radiance values which have physical meaning. The linear transformation equation is as follows:

$$L_\lambda = \frac{DN_\lambda}{\alpha_\lambda}. \tag{9}$$

Geomorphometric parameters were also generated from the DEM. Specifically, slope angle (β_τ) and slope-aspect angles (θ_τ) were characterized as

$$f_x = \frac{\partial z}{\partial x}, f_y = \frac{\partial z}{\partial y}, \tag{10}$$

$$\beta_t = \arctan \sqrt{f_x^2 + f_y^2}, \tag{11}$$

and

$$\phi_t = \arctan \left[\frac{f_y}{f_x} \right]. \tag{12}$$

These topographic parameters were used to produce a $\cos i$ image that was used to generate results from the Cosine-correction and Minnaert-correction procedures.

4.4 Anisotropic-Reflectance Correction

Two ARC approaches were tested for their ability to reduce the topographic effect in satellite imagery. If we assume that surface reflectance is isotropic and that the local topography is primarily responsible for the topographic effect, we might be able to use the Cosine-correction method to reduce the topographic effect. This is represented as

$$L_\lambda^n = \frac{L_\lambda}{\cos i}, \tag{13}$$

where L_λ^n is the normalized radiance after ARC, and L_λ represents the at-satellite radiance. The local influence of the topography is accounted for by $\cos i$, as this is proportional to the direct solar irradiance reaching the surface.

If we assume that surface reflectance is anisotropic, we can use and evaluate the Minnaert correction procedure for reducing the topographic effect in satellite imagery. This

correction procedure attempts to characterize anisotropic reflectance and accounts for the exitant angle (e), which is equivalent to the slope of the terrain for nadir viewing sensors. The transformation procedure is

$$L_\lambda^n = (L_\lambda \cos e)/(\cos^{k_\lambda} i \cos^{k_\lambda} e), \tag{14}$$

where k is the Minnaert constant that ranges from $0.0 - 1.0$. The coefficient is not a true constant, but attempts to characterize the departure of reflectance from that of a Lambertian surface (i.e., isotropic reflectance). A k value of 1 indicates isotropic reflectance. A lower coefficient represents departure from this and indicates the degree of anistrophy. It is also important to note that k is wavelength dependent.

In general, the calculation of k values is accomplished using least-squares regression analysis. To calculate k values, a regression analysis is performed on the variables x and y, where $x = \log(\cos i \cos e)$ and $y = \log(L_\lambda \cos e)$. The slope of the regression equation (β_r) is then used to represent k, such that $k = \beta_r$.

One way to evaluate the Minnaert correction procedure is to compute a global k value for an image. This approach assumes that the anisotropic nature of reflectance is homogeneous over the study area. We might suspect that this assumption is invalid, and that topographic and land-cover variations would cause k to vary spatially, such that a global value would not produce spatially consistent results. Numerous investigators, however, have indicated that this approach can reduce the topographic effect in satellite imagery. Consequently, this approach was evaluated.

It seems more reasonable to assume that the local influence of topography and land

cover would produce highly variable patterns of anisotropic reflectance. Given this assumption, an approach using a local window analysis generated a unique k value for each pixel, based upon a regression analysis of the data. Various window sizes were evaluated to determine what effect window size would have on the analysis. Windows sizes were arbitrarily selected to represent analysis of local to more regional scales (i.e., $11 \times 11, 21 \times 21, 101 \times 101, 201 \times 201$). With this systematic approach, the normalization procedure will have N k values, where $N = (n_l - (p + p))(n_c - (p + p))$. N is a function of the number of lines (n_l) and the number of columns (n_c) in the image. It is also a function of the window size (w), where $p = int(w/2.0)$. This implementation also enabled the production of k value images and r^2 images resulting from regression analysis for data in each window. By generating these data sets, it was possible to assess the validity of the regression analysis and examine anisotropic-reflectance characteristics throughout the entire region.

It is also reasonable to assume that specific land-cover classes exhibit a strong influence on anisotropic reflectance such that the effective reduction of the topographic effect requires characterization of anisotropic reflectance for specific land-cover classes. To test this, an image segmentation approach was investigated. The fundamental land-cover structure within the scene was produced using NIR image thresholding and the ISODATA clustering algorithm on a NIR/RED ratio image, which reduced the influence of the topographic effect, and enabled vegetation to be classified. This resulted in a map of three classes of land cover for Nanga Parbat. (Figure 13).

Snow, vegetation, and non-vegetation features were easily mapped at Nanga Parbat, and these land-cover classes are known to exhibit different anisotropic-reflectance characteristics because of their unique biophysical properties (Duguay and LeDrew, 1992; Hugli and Frei, 1983). It is important to note that the purpose of the classification is not to accurately map these features, but to segment the image into regions so that three k values can be computed which characterize the influence of land cover on anisotropic reflectance. If this approach is valid, then it is possible to segment the image after ARC to produce more accurate classification results. This in turn can be used to produce better ARC results, and so on. This would increase the number of k values that would be used for ARC, and theoretically improve anisotropic-reflectance characterization. Ultimately, the validity of using computed k values and producing meaningful results rests on the statistical significance (high r^2 values) of the computed k values. A k value generated from regression analysis with a low r^2 indicates that the k value does not accurately characterize anisotropic reflectance (Bishop and Colby, 2002).

4.5 Evaluation of Results

Normalized imagery was visually interpreted and compared to the original NIR image to determine if there was a reduction in the topographic effect. While this evaluation procedure is frequently used, it does not represent an effective way to determine the validity of ARC results. It was used in this study to provide insight into the influence of various ARC approaches and was compared to results of the quantitative analysis, as various statistics

that characterized the results required further interpretation.

Basic descriptive statistics were generated for the original and normalized imagery. This was done to compare the magnitude of radiance values in imagery, and to determine if the ARC procedures altered the global variance structure, such that information compression occurred, or anomalous values were generated. Scatterplots were generated comparing the original image and normalized image data to $\cos i$ values to understand the relationships between reflectance, topography, and the direct-irradiance component.

The topographic effect should produce a strong linear or non-linear relationship between NIR reflectance and $\cos i$ values, as the local topography and solar geometry dictates a strong correlation between irradiance and reflectance. In theory, successful ARC should reduce or remove the topographic effect, such that the slope of the regression line for normalized radiance should approach zero and the strength of the relationship be equivalent to $r^2 = 0.0$. This approach to evaluating ARC results has been used by a variety of investigators. If a pattern or relationship between normalized radiance and $\cos i$ were found, this would indicate a topographic influence in the normalized data.

This approach can be used to determine if there is a local topographic influence found in the normalized data. It does not, however, assess the spatially dependent variance in the normalized data which is influenced by topography and land cover. We might not expect any change in the global variance structure of the original imagery compared to the normalized imagery, although there might be a difference if an ARC procedure performs very poorly. We might, however, expect the influence of anisotropic reflectance to occur at

various scales that are controlled by the spatial structure of land cover and the topographic characteristics of the area. Given this scenario, the topographic effect would occur at a variety of scales. For example, within shadowed areas that exhibit spectrally distinct land cover features, a good ARC procedure should increase variance. Conversely, in shadowed homogeneous areas, spectral variance may not increase or decrease. Furthermore, at the landscape scale, spectral variance could increase, decrease, or remain the same, depending upon the conditions of land cover, topography and solar geometry. This indicates that a rigorous evaluation of ARC results requires an examination and comparison of the spatially dependent variance structure of the original and normalized images. Geostatistical techniques can be used to accomplish this.

Numerous subareas over Nanga Parbat were selected to further evaluate ARC results for areas of homogeneous and heterogeneous land cover (Figure 14). For these areas, descriptive statistics and scatterplots of radiance and $\cos i$ were generated and compared.

Two-dimensional semivariogram analysis was also conducted, where every pixel was compared to every other pixel in a subarea. Within an $n_x \times n_y$ grid there will be N point pairs, where $N = n_x^2(n_y^2 - 1)/2$. The variance component is $\Delta L = (L_1 - L_2)^2$, and the horizontal distance is $\Delta x = [(x_1 - x_2)^2 + (y_1 - y_2)^2]^{0.5}$. I summed the variance over a binned horizontal distance interval (20 m) and divided this by the number of observations within each bin to calculate the average semivariance ($\overline{S}^2$).

Effective ARC should result in a normalized radiance image that exhibits less spectral variation at lag distances where topography increases spectral variability, and greater

spectral variation at lag distances associated with land-cover variation. Bishop and Colby (2002) were the first to perform this rigorous evaluation of ARC results.

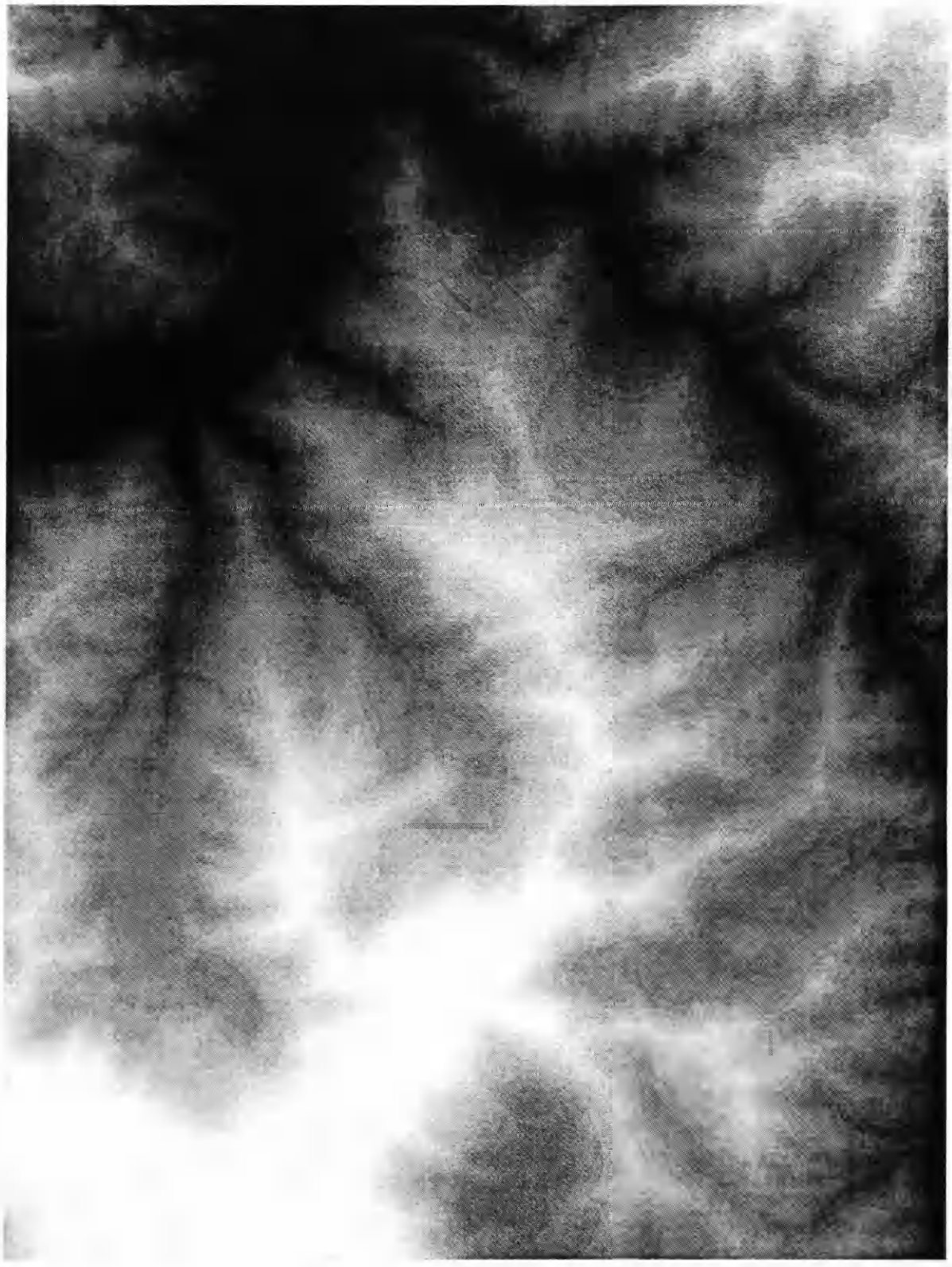

Figure 11: A digital elevation model for a part of Nanga Parbat (Each pixel represents 20 meters by 20 meters).

Figure 12: SPOT-3 NIR orthorectified image of Nanga Parbat.

Figure 13: Landcover classificaton map of the Nanga Parbat area. Black represents non-vegetation, intermediate gray represents vegetation on the landscape, and light gray represents snow cover at higher altitudes.

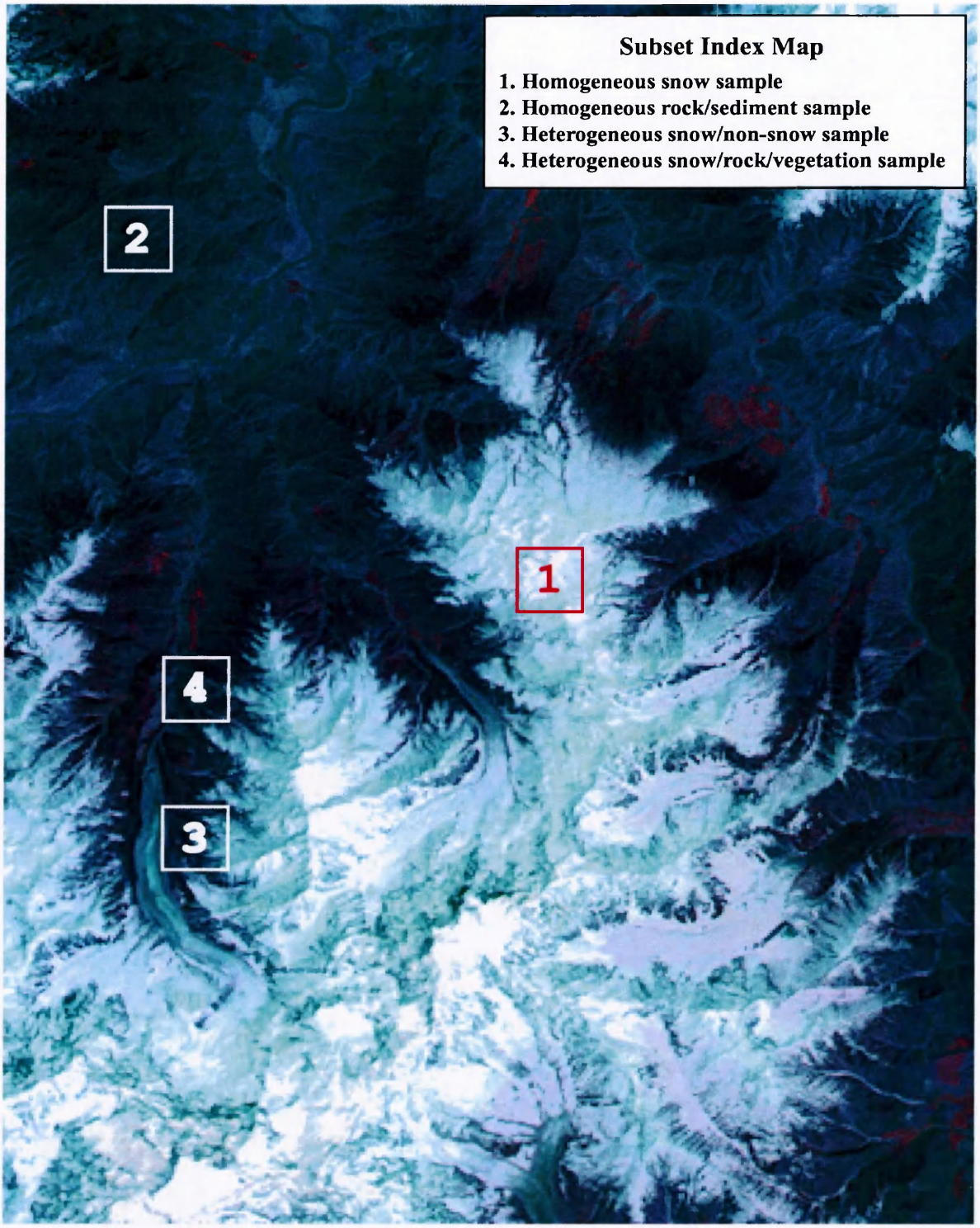

Figure 14: Sample locations at Nanga Parbat.

5 Results

5.1 Anisotropic-Reflectance Correction

Each ARC approach was evaluated to determine if it appropriately normalized the NIR image to account for the irradiant and radiant flux caused by the topography and land cover. Visual interpretation results were compared to results of statistical analysis to evaluate the spectral variance in each normalized image.

It was evident that Cosine correction cannot be used for normalization in terrain that exhibits extreme relief and steep slopes (Figure 15). The approach produces high radiance values throughout the image regardless of land cover. Large radiance values were found wherever there were steep slopes. This overcorrection is most evident in the Raikot Fault zone where active river incision and uplift generate steep slopes and "V" shaped valleys. Overcorrection also occured at high altitudes along the knife-edged ridge, where glacier erosion and active uplift generate steep headwalls.

The overcorrection was associated with low $\cos i$ values. Steep slopes decrease the direct solar irradiance (low $cosi$ values) which caused overcorrection. This result indicated that the method needs to account for other irradiance components (E^d and E^T) so that overcorrection does not occur. In practice, it is very difficult to accomplish this, as detailed physical modeling is required to estimate these irradiance components.

The Minnaert-correction procedure, using a global Minnaert constant, appeared to produce better results (Figure 16). Spectral variation caused by the topography was dramat-

ically reduced. Furthermore, overcorrection was dramatically reduced, compared to the cosine-corrected normalized image.

Figure 15: SPOT-3 NIR normalized image using the Cosine-correction method. High radiance values (overcorrection) is the result of steep slopes and relatively low direct solar irradiance.

Close examination of the normalized image, however, indicated that the procedure produced high radiance values (overcorrection) for some pixels. These pixels exhibited very steep slopes and were found at the base of the steepest slopes in the Raikot Fault zone and at high altitude along the headwalls. This indicated that although the use of a non-Lambertian reflectance model reduced spectral variation caused by the topography, the method has its limitations as the other irradiant-flux components must be accounted for.

The global regression analysis yielded a k and r^2 value of 0.5234 and 0.123 respectively. These results indicated that this implementation did not accurately characterize anisotropic reflectance (the magnitude of the departure from Lambertian reflectance), as the regression analysis did not result in the explanation of the spectral variance (i.e., low r^2 value). Consequently, one k value cannot be used to account for anisotropic reflectance caused by land cover.

The Minnaert-correction procedure, based upon land-cover stratification, produced statistically valid Minnaert constants, such that the topography and land-cover influences on reflectance were taken into consideration (Table 2). The resulting normalized image (Figure 17) is very comparable to the previous implementation, in that spectral variation appears to be effectively normalized. It is important to note that a few overcorrected areas were found in the image. This indicated that even though the k values were statistically valid, the irradiant flux must be better characterized so that overcorrection does not occur. Visual interpretation alone cannot fully resolve the degree to which overcorrection occurs in normalized images.

Table 2: Results of land cover stratified-regression analysis.

Class	k	r^2	n
Non-vegetation	0.4052	0.4081	1266086
Vegetation	0.4437	0.5182	418362
Snow/Firn	0.4840	0.5757	958465

The Minnaert-correction procedure based upon window analysis, produced images that appeared to be very comparable to each other and the previous normalized images based on the Minnaert-correction procedure (Figures 18-21). The topographic effect appeared to be reduced, although overcorrection can be seen in each image, indicating the reoccurring problem of addressing the irradiant flux in complex terrain. Window-based analysis results provided more insight into the effectiveness of this implementation approach for ARC.

Figure 16: SPOT-3 NIR normalized image using the Minnaert-correction procedure based upon a global Minnaert constant.

Figure 17: SPOT-3 NIR normalized image using multiple Minnaert constants that were computed based upon land-cover stratification.

Figure 18: SPOT-3 NIR normalized image using the Minnaert-correction procedure and multiple Minnaert constants based upon window analysis (11x11 pixel window).

Figure 19: SPOT-3 NIR normalized image using the Minnaert-correction procedure and multiple Minnaert constants based upon window analysis (21x21 pixel window).

Figure 20: SPOT-3 NIR normalized image using the Minnaert-correction procedure and multiple Minnaert constants based upon window analysis (101x101 pixel window).

Figure 21: SPOT-3 NIR normalized image using the Minnaert-correction procedure and multiple Minnaert constants based upon window analysis (201x201 pixel window).

It is important to note that k values must range from $0.0 - 1.0$ and characterize the degree of anistropy as it departs from Lambertian ($k = 1.0$). Examination of window-based results indicated that small window sizes did not produce acceptable k values, as the magnitude is outside the range of permissible values, and negative relationships produce invalid values (Table 3). Small window sizes resulted in a high degree of variation in k values. Larger window sizes resulted in less variation, although the 101 window size resulted in k values greater than 1.0. This result indicated that smaller window sizes cannot be used to accurately characterize anisotropic reflectance, as positive and negative relationships can occur, and are the result of changing land cover and topographic conditions. As the window size increased, more topographic variation was accounted for, which resulted in a regression analysis that generated k values in the proper range.

Table 3: Descriptive statistics of the slope of the regression line (k) for window-based regression analysis.

	1 [a]	2 [b]	3 [c]	4 [d]
Min	-16.7260	-4.1442	0.1082	0.1705
Max	12.1720	4.1077	1.8743	1.0010
Median	0.4366	0.4769	0.5229	0.5435
Mean	0.5200	0.5460	0.5560	0.5510
STD	0.3500	0.2670	0.1560	0.1090
Range	28.8980	8.2519	1.7660	0.8305

[a]NLM11 - Minnaert correction (11 x 11 pixel window)
[b]NLM21 - Minnaert correction (21 x 21 pixel window)
[c]NLM101 - Minnaert correction (101 x 101 pixel window)
[d]NLM201 - Minnaert correction (201 x 201 pixel window)

These results must be compared with the r^2 statistics of regression analysis (Table 4). For all window sizes, r^2 values ranged from very low to very high. This is problematic, as

Table 4: Descriptive statistics of the coefficient of determination (r^2) from window-based regression analysis.

	1 [a]	2 [b]	3 [c]	4 [d]
Min	$1.59\times10^{-}11$	$2.07\times10^{-}11$	0.0060	0.0124
Max	0.9940	0.9836	0.8813	0.8391
Median	0.5818	0.5792	0.5434	0.4746
Mean	0.5390	0.5410	0.5050	0.4620
STD	0.2630	0.2280	0.1990	0.2000
Range	0.9940	0.9836	0.8753	0.8267

[a]NLM11 - Minnaert correction (11 x 11 pixel window)
[b]NLM21 - Minnaert correction (21 x 21 pixel window)
[c]NLM101 - Minnaert correction (101 x 101 pixel window)
[d]NLM201 - Minnaert correction (201 x 201 pixel window)

high r^2 values are required so that statistically valid k values are used for normalization. In general, higher r^2 values were obtained for smaller window sizes, although invalid k values result. Visual interpretation of r^2 images provided additional information about the validity of this Minnaert-correction implementation.

Low r^2 values are associated with areas on the landscape that exhibit shallow slopes, such as floodplains, modern alpine glaciers, erosional and depositional surfaces at altitude which are the result of glaciation, and large landslides (Figure 22). It is also important to note the high spatial variability of r^2 values. In general, the same results were obtained for the 21 $\times$ 21 window (Figure 23), although r^2 values were more spatially homogeneous due to the larger window size. These results indicated that small window sizes do not account for topographic variation as it relates to the irradiant and radiant flux, which is why window-based regression analysis produced invalid Minnaert Constants.

Figure 22: Coefficient of determination (r^2) image based upon regression analysis for a 11×11 pixel window.

Figure 23: Coefficient of determination (r^2) image based upon regression analysis for a 21×21 pixel window.

Figure 24: Coefficient of determination (r^2) image based upon regression analysis for a 101×101 pixel window.

Figure 25: Coefficient of determination (r^2) image based upon regression analysis for a 201×201 pixel window.

5.2 Global Statistical Analysis

Examination of the regression results for the larger window sizes indicated statistically valid results for pixels representing homogeneous land cover classes, and low r^2 values for pixels when multiple land-cover classes were found within a window (Figures 24 and 25). This resulted in the highlighting of the snow-non-snow boundary, as different land-cover classes exhibit unique anisotropic-reflectance characteristics. Collectively, these results indicated that an optimal window size must be selected, based upon a user's knowledge of the topography and land cover. The window must be large enough to account for topographic variation, and small enough not to include multiple land-cover classes. This is problematic, as mountain environments can be very heterogeneous, and the selection of an optimal window size that meets this criteria is difficult. In addition, there will always be the possibility of multiple land-cover classes in a local area as the window size increases.

Statistical analysis confirmed the interpretations based upon visual examination of the normalized imagery. Every ARC procedure produced maximum radiance values that did not fall within acceptable radiance ranges for the highest reflective features (Table 5). In general, normalized imagery exhibited higher spectral variation than the original NIR image. This was caused by overcorrection.

It is generally assumed that effective ARC decreases the global spectral variance (reduction of spectral variance caused by the topography). This overly simplistic assumption, if used, would indicate that the best results were obtained using the local, window-based implementation of the Minnaert correction procedure (small window sizes). These images

Table 5: Summary statistics for SPOT-3 NIR image and normalized imagery.

Image	Min	Max	Median	Mean	STD	Range
NIR [a]	17.7300	300.24	85,393	120.9470	62.5050	282.51
Cosine [b]	19.6960	2.48×10^7	118.820	401.1790	55958.03	2.48×10^7
NLMG [c]	18.6870	50879	90.4160	128.6360	144.6570	50860.31
NLM3 [d]	17.9470	26399	78.2160	123.1870	86.6230	26381.05
NLM11 [e]	15.7560	594.79	89.2370	125.5130	66.7970	579.03
NLM21 [f]	14.0770	2301.3	89.5060	127.3020	68.0190	2287.22
NLM101 [g]	14.0400	81927	89.0960	129.9270	119.4220	81912.96
NLM201 [h]	15.9190	94817	90.9110	130.8990	185.4260	94801.08

[a]NIR - SPOT-3 NIR Image.
[b]Cosine -normalized NIR image (Cosine correction).
[c]NLMG - Normalized NIR image (Minnaert correction and global Minnaert constant).
[d]NLM3 - Normalized NIR image (Minnaert correction and land-cover stratification).
[e]Nlm11 - Normalized NIR image (Minnaert Correction and 11 x 11 pixel window).
[f]Nlm21 - Normalized NIR image (Minnaert Correction and 21 x 21 pixel window).
[g]Nlm101 - Normalized NIR image (Minnaert Correction and 101 x 101 pixel window).
[h]Nlm201 - Normalized NIR image (Minnaert Correction and 201 x 201 pixel window).

(Figures 18 and 19) exhibit the smallest global variance. This result must be interpreted with respect to invalid k values which effectively compress the variance, given the range of k. This resulted in normalized imagery that appeared to reduce the spectral variation caused by topography. In essence, however, the k values did not adequately characterize anisotropic reflectance over the entire scene.

It is more realistic to assume that effective ARC will result in an increase or a decrease in spectral variance, depending upon the topographic and land-cover complexities of a particular area. This assumption dictates that global statistical analysis of normalized imagery should be ineffective as a diagnostic tool to evaluate ARC procedures, as effective normalization may increase spectral variation is some areas, while decreasing spectral variation in others. The net global effect may in fact be an overall increase or decrease in global

variance depending upon the landscape complexity. Scale-dependent analysis of variance, therefore, is required to identify changes in spectral variance related to land cover.

5.3 Diagnostic Analysis

Four subimages were selected to evaluate the spectral variance for two homogeneous areas (samples 1 and 2) and two heterogeneous areas (samples 3 and 4). Effective ARC should result in a decrease in spectral variation over homogeneous land cover areas and increased spectral variation over heterogeneous land cover areas.

5.3.1 Homogeneous Rock/Sediment Sample

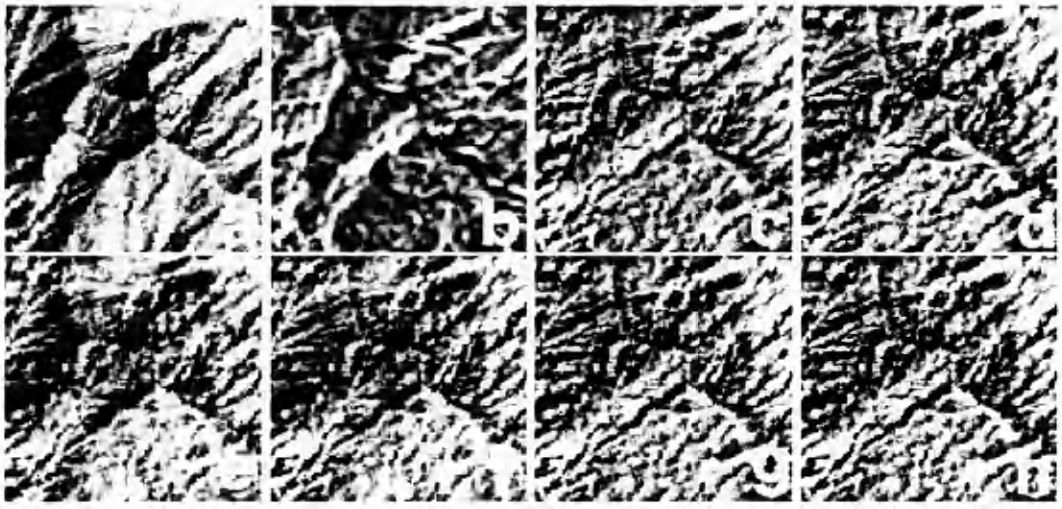

Figure 26: Subimage of relating homogeneous land cover north of the Indus River. (a) NIR - SPOT-3 NIR image (b) Cosine - Normalized NIR image (Cosine correction) (c) NLMG - Normalized NIR image (Cosine correction and a global Minnaert constant) (d) NLM3 - Normalized NIR image (Minnaert correction and land-cover stratification) (e) NLM11 - Normalized NIR image (Minnaert correction and 11 x 11 pixel window) (f) NLM21 - Normalized NIR image (Minnaert correction and 21 x 21 pixel window) (g) NLM101 - Normalized NIR image (Minnaert correction and 101 x 101 pixel window) (h) NLM201 - Normalized NIR image (Minnaert correction and 201 x 201 pixel window)

Based upon visual interpretation, it was difficult to determine which procedure produced the best result, although the spectral variance caused by the topography should be reduced(Figure 26). All the ARC procedures, except the Cosine-correction method, appeared to reduce the spectral variation. Statistical analysis supported this interpretation as the spectral variance for all Minnaert correction implementations are less than the original NIR image (Table 6).

Table 6: Summary statistics for sample 1 in Figure 26.

Image	Min	Max	Mean	STD
NIR [a]	41.3711	85.1063	67.1379	6.5900
Cosine [b]	48.5830	300.0326	89.0022	19.5030
NLMG [c]	43.7306	100.7105	69.7585	5.4777
NLM3 [d]	42.4840	85.6099	65.6783	5.0412
NLM11 [e]	41.9205	96.1164	67.6383	5.8044
NLM21 [f]	43.1197	90.3212	67.5664	5.4468
NLM101 [g]	43.2123	89.5158	67.4759	5.1505
NLM201 [h]	42.9763	91.3130	67.3810	5.0743

[a]NIR - SPOT-3 NIR Image.
[b]Cosine -normalized NIR image (Cosine correction).
[c]NLMG - Normalized NIR image (Minnaert correction and global Minnaert constant).
[d]NLM3 - Normalized NIR image (Minnaert correction and land-cover stratification).
[e]Nlm11 - Normalized NIR image (Minnaert Correction and 11 x 11 pixel window).
[f]Nlm21 - Normalized NIR image (Minnaert Correction and 21 x 21 pixel window).
[g]Nlm101 - Normalized NIR image (Minnaert Correction and 101 x 101 pixel window).
[h]Nlm201 - Normalized NIR image (Minnaert Correction and 201 x 201 pixel window).

Cosine correction was the exception, as overcorrection caused the spectral variance to be higher (Figure 27). The Minnaert-correction procedure (global Minnaert constant) also produced high radiance values (Figure 28).

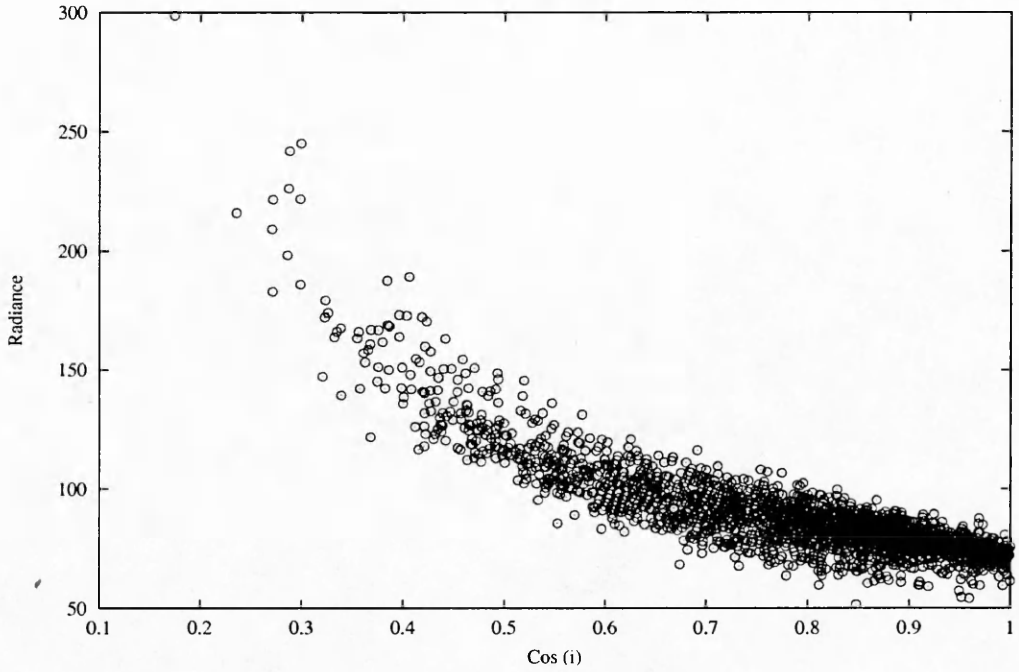

Figure 27: Scatterplot of the relationship between the Cosine-corrected normalized radiance and $\cos i$. Normalized radiance values systematically increased with decreasing $\cos i$.

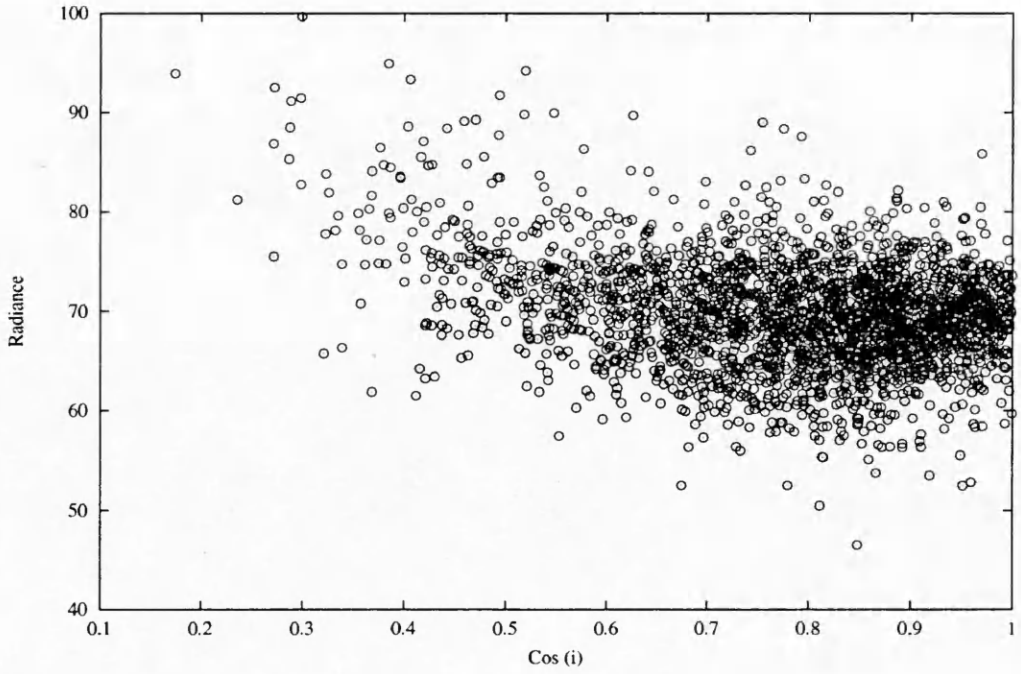

Figure 28: Scatterplot of the relationship between the Minnaert-corrected (global k) normalized radiance and $\cos i$. The relationship is similar to Figure 27 in that overcorrection occurs for pixels exhibiting low $\cos i$ values.

Semivariogram analysis indicated that the land-cover stratification approach produced the best normalized subimage, as the spatially dependent, spectral variation was smaller at various lag distance compared to the other ARC approaches (Figure 29).

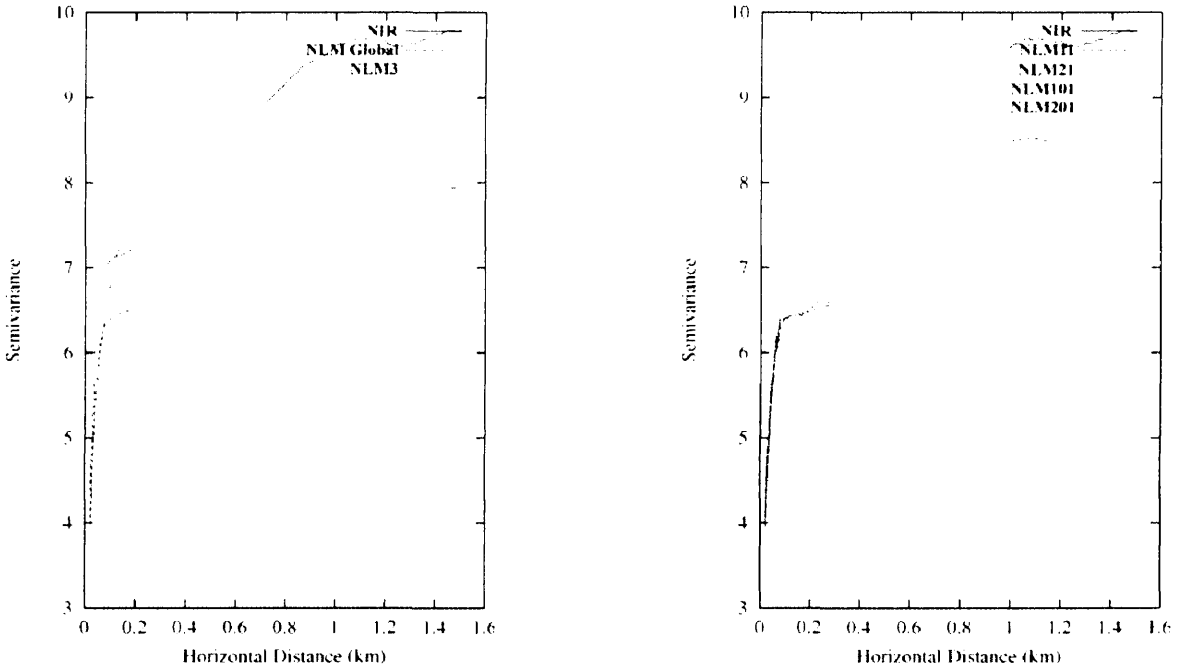

Figure 29: Two-dimensional semivariograms for sample one. All ARC procedures decrease the spatially-dependent variance. The Minnaert-correction procedure based upon land-cover stratification produced the best result. (NIR) - SPOT3 NIR image, (NLM Global) - Normalized NIR image (Minnaert correction and global Minnaert constant), (NLM3) - Normalized NIR image (Minnaert correction and land-cover stratification), (NLM11) - Normalized NIR image (Minnaert correction and 11 x 11 pixel window), (NLM21) - Normalized NIR image (Minnaert correction and 21 x 21 pixel window), (NLM101) - Normalized NIR image (Minnaert correction and 101 x 101 pixel window), (NLM201) - Normalized NIR image (Minnaert correction and 201 x 201 pixel window).

5.3.2 Homogeneous Snow Sample

Sample two subimages represent snow cover at high altitude (Figure 30). The cosine correction procedure significantly overcorrected, and high radiance values were also found for the global and window-based implementations of the Minnaert-correction procedure (Figures 31 and 32).

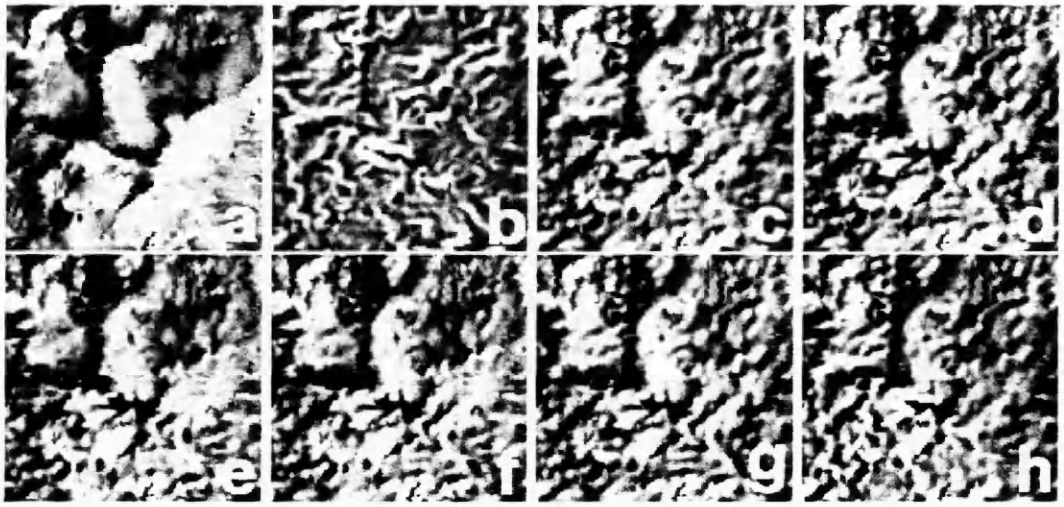

Figure 30: Subimage of snow cover at high altitude. (a) NIR - SPOT-3 NIR image (b) Cosine - Normalized NIR image (Cosine correction) (c) NLMG - Normalized NIR image (Cosine correction and a global Minnaert constant) (d) NLM3 - Normalized NIR image (Minnaert correction and land-cover stratification) (e) NLM11 - Normalized NIR image (Minnaert correction and 11 x 11 pixel window) (f) NLM21 - Normalized NIR image (Minnaert correction and 21 x 21 pixel window) (g) NLM101 - Normalized NIR image (Minnaert correction and 101 x 101 pixel window) (h) NLM201 - Normalized NIR image (Minnaert correction and 201 x 201 pixel window).

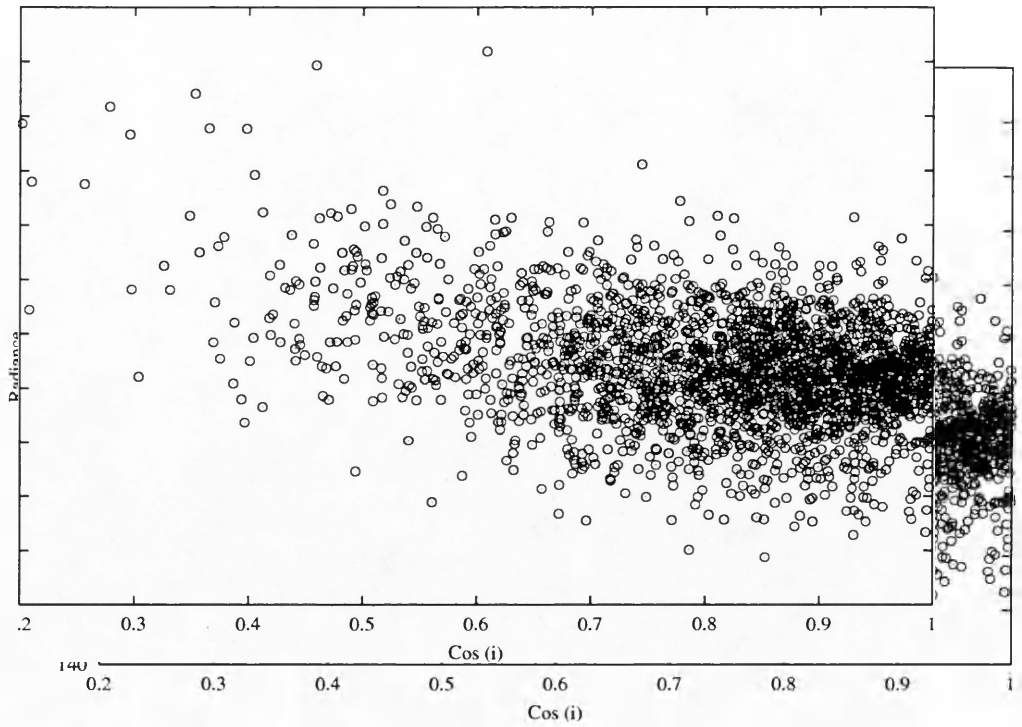

Figure 31: Scatterplot of relationship between the Minnaert-corrected (global k) normalized radiance and $\cos i$.

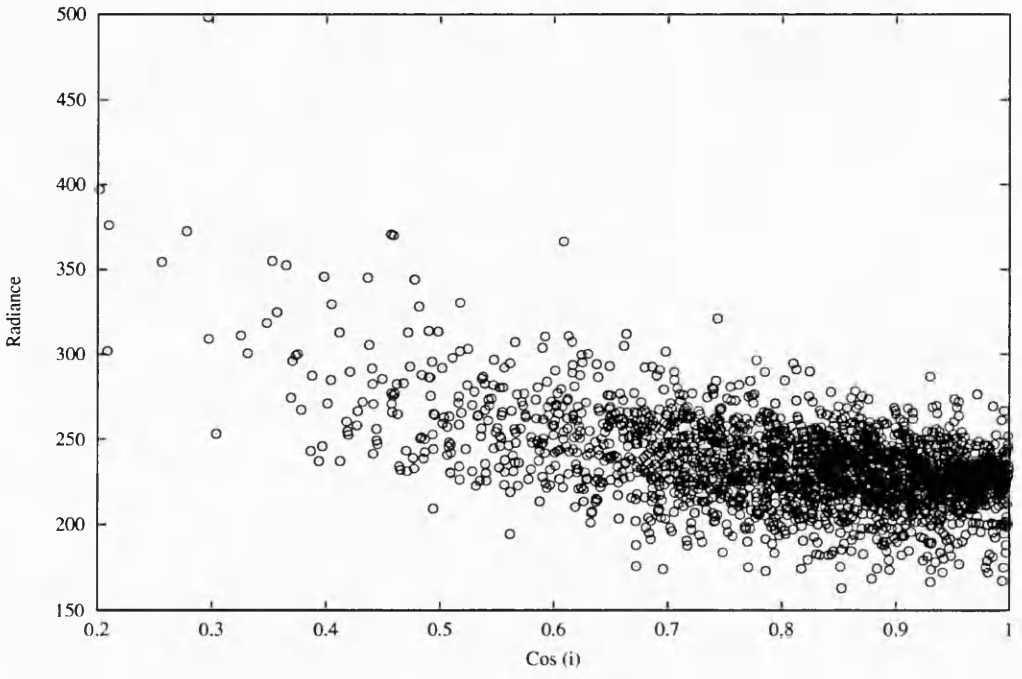

Figure 32: Scatterplot of the relationship between the Minnaert-corrected (201×201 pixel window) normalized radiance and $\cos i$.

Statistical analysis of the subscene indicated that all procedures resulted in an increase in spectral variance. It was anticipated that ARC would have decreased the spectral variance (Table 7).

Table 7: Statistics for sample 2.

Image	Min	Max	Mean	STD
NIR [a]	143.0260	300.2364	217.2873	18.3440
Cosine [b]	165.7823	1359.6949	274.4012	63.8324
NLMG [c]	139.9285	384.9571	227.2528	20.5690
NLM3 [d]	134.1826	345.0351	223.2186	19.5467
NLM11 [e]	135.0404	326.8943	221.5523	20.3175
NLM21 [f]	140.2734	330.3584	222.6164	19.6084
NLM101 [g]	133.7084	381.8048	222.7164	19.6595
NLM201 [h]	153.1408	498.4654	234.4161	24.7572

[a]NIR - SPOT-3 NIR Image.
[b]Cosine -normalized NIR image (Cosine correction).
[c]NLMG - Normalized NIR image (Minnaert correction and global Minnaert constant).
[d]NLM3 - Normalized NIR image (Minnaert correction and land-cover stratification).
[e]Nlm11 - Normalized NIR image (Minnaert Correction and 11 x 11 pixel window).
[f]Nlm21 - Normalized NIR image (Minnaert Correction and 21 x 21 pixel window).
[g]Nlm101 - Normalized NIR image (Minnaert Correction and 101 x 101 pixel window).
[h]Nlm201 - Normalized NIR image (Minnaert Correction and 201 x 201 pixel window).

Semivariogram analysis also indicated that there was an increase in the spectral variance at all lag distances for each ARC procedure (Figure 33). This can be potentially explained if the subarea does not represent a truly homogeneous sample of snow. At altitude, the steep slopes and blowing wind can remove snowcover, such that bare rock is exposed in this high-altitude snow zone. If this is the case, then ARC would actually increase the spatially dependent spectral variance such that effective ARC would enhance the spectral differences between snow and rock, thereby accounting for an increase in spectral variance.

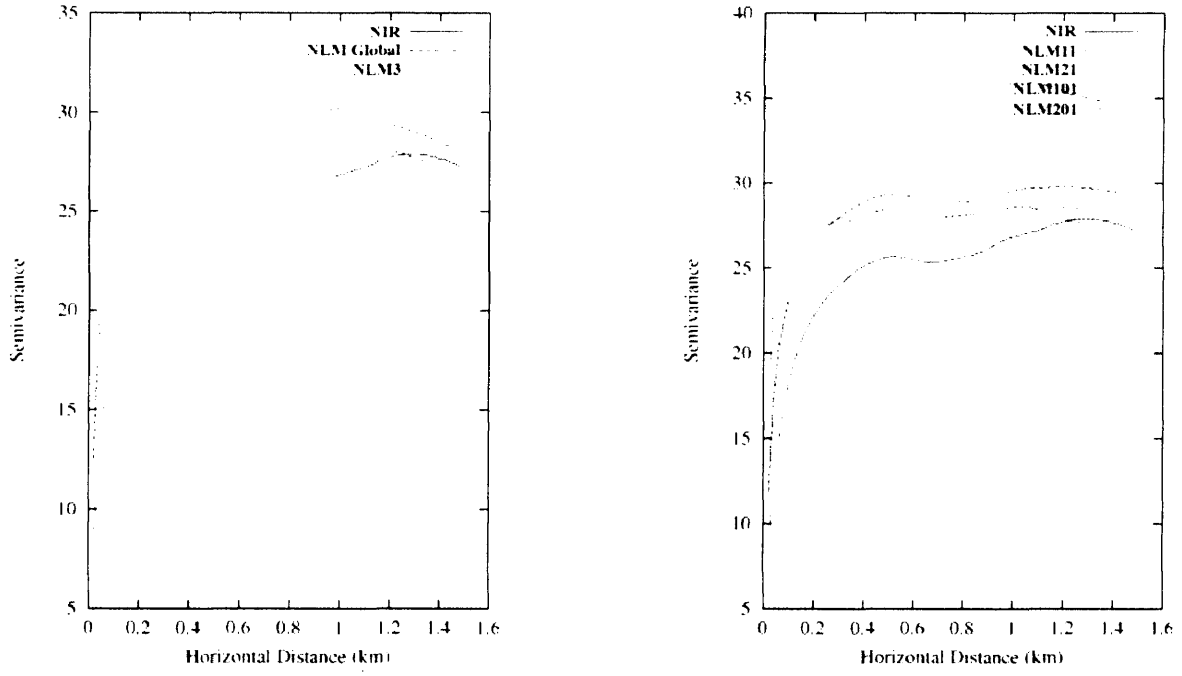

Figure 33: Two-dimensional semivariograms for sample two. (NIR) - SPOT3 NIR image, (NLM Global) - Normalized NIR image (Minnaert correction and global Minnaert constant), (NLM3) - Normalized NIR image (Minnaert correction and land-cover stratification), (NLM11) - Normalized NIR image (Minnaert correction and 11 x 11 pixel window), (NLM21) - Normalized NIR image (Minnaert correction and 21 x 21 pixel window), (NLM101) - Normalized NIR image (Minnaert correction and 101 x 101 pixel window), (NLM201) - Normalized NIR image (Minnaert correction and 201 x 201 pixel window).

5.3.3 Heterogeneous Snow/Non-Snow Sample

Sample three subimages represent a heterogeneous, land-cover mixture of snow and non-snow classes (Figure 34). Statistical analysis indicated that the spectral variance for normalized images was greater that the variance in the original NIR subimage (Table 8).

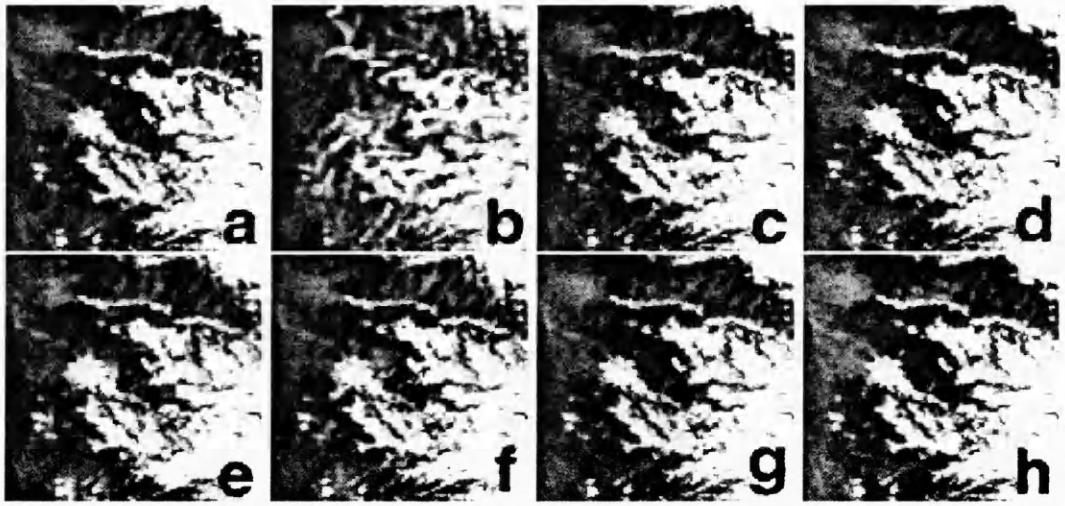

Figure 34: Subimage of heterogeneous land cover. (a) NIR - SPOT-3 NIR image (b) Cosine - Normalized NIR image (Cosine correction) (c) NLMG - Normalized NIR image (Cosine correction and a global Minnaert constant) (d) NLM3 - Normalized NIR image (Minnaert correction and land-cover stratification) (e) NLM11 - Normalized NIR image (Minnaert correction and 11 x 11 pixel window) (f) NLM21 - Normalized NIR image (Minnaert correction and 21 x 21 pixel window) (g) NLM101 - Normalized NIR image (Minnaert correction and 101 x 101 pixel window) (h) NLM201 - Normalized NIR image (Minnaert correction and 201 x 201 pixel window).

This was expected, although the increased variance was caused by overcorrection. Semivariogram analysis indicated that all the Minnaert-correction implementations increased the spectral variance normalization using the-land cover stratification implementation produced the best results (Figure 35).

Table 8: Summary statistics for sample three.

Image	Min	Max	Mean	STD
NIR [a]	39.0070	203.3096	93.7808	35.0714
Cosine [b]	55.9246	1774.4891	148.6921	82.1787
NLMG [c]	43.3671	282.7252	107.1405	42.6549
NLM3 [d]	34.9880	232.9450	101.2887	41.2255
NLM11 [e]	38.8379	318.0933	101.5012	38.8477
NLM21 [f]	37.0504	267.1944	102.3408	37.9405
NLM101 [g]	32.7867	256.2081	100.2029	42.3113
NLM201 [h]	27.4631	211.4338	91.3902	36.3283

[a]NIR - SPOT-3 NIR Image.
[b]Cosine -normalized NIR image (Cosine correction).
[c]NLMG - Normalized NIR image (Minnaert correction and global Minnaert constant).
[d]NLM3 - Normalized NIR image (Minnaert correction and land-cover stratification).
[e]Nlm11 - Normalized NIR image (Minnaert Correction and 11 x 11 pixel window).
[f]Nlm21 - Normalized NIR image (Minnaert Correction and 21 x 21 pixel window).
[g]Nlm101 - Normalized NIR image (Minnaert Correction and 101 x 101 pixel window).
[h]Nlm201 - Normalized NIR image (Minnaert Correction and 201 x 201 pixel window).

5.3.4 Heterogeneous Snow/Rock/Vegetation Sample

For more complicated subscenes, visual interpretation and Statistical analysis indicated that all ARC procedures increased the spectral variance in the normalized images (Figure 36 and Table 9). The increased variance in the Cosine-corrected and global Minnaert-corrected images was caused by overcorrection. Semivariogram analysis revealed that all Minnaert-correction implementations increased the spectral variance, although the window-based implementations produced greater spectral differentiation between land-cover classes (Figure 37).

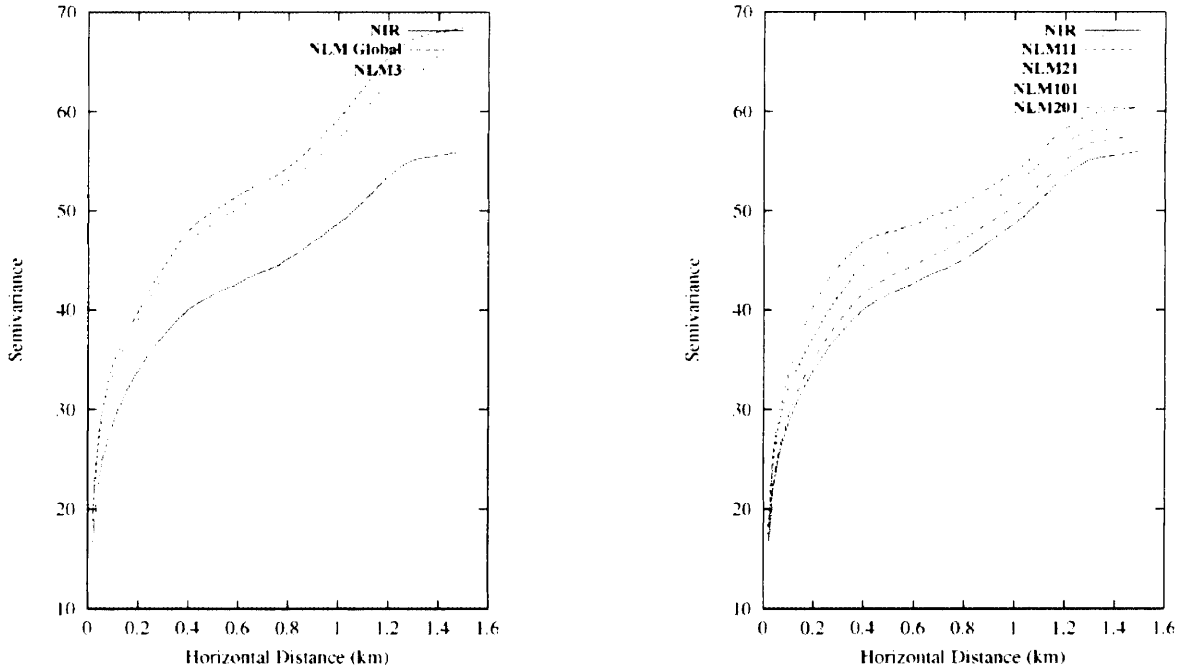

Figure 35: Two-dimensional semivariograms for sample three. (NIR) - SPOT3 NIR image, (NLM Global) - Normalized NIR image (Minnaert correction and global Minnaert constant), (NLM3) - Normalized NIR image (Minnaert correction and land-cover stratification), (NLM11) - Normalized NIR image (Minnaert correction and 11 x 11 pixel window), (NLM21) - Normalized NIR image (Minnaert correction and 21 x 21 pixel window), (NLM101) - Normalized NIR image (Minnaert correction and 101 x 101 pixel window), (NLM201) - Normalized NIR image (Minnaert correction and 201 x 201 pixel window).

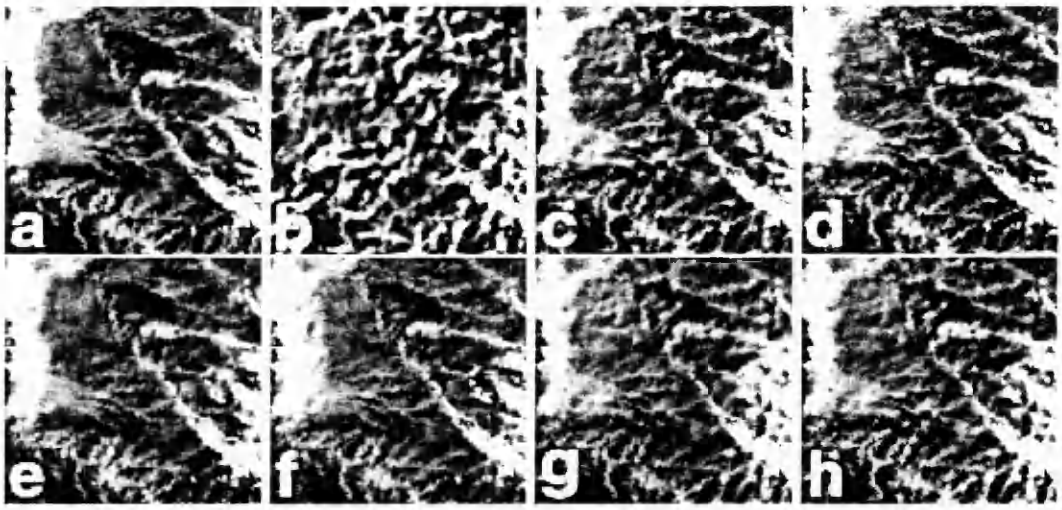

Figure 36: Subimage of heterogeneous land cover in the Raikot Basin. (a) NIR - SPOT-3 NIR image (b) Cosine - Normalized NIR image (Cosine correction) (c) NLMG - Normalized NIR image (Cosine correction and a global Minnaert constant) (d) NLM3 - Normalized NIR image (Minnaert correction and land-cover stratification) (e) NLM11 - Normalized NIR image (Minnaert correction and 11 x 11 pixel window) (f) NLM21 - Normalized NIR image (Minnaert correction and 21 x 21 pixel window) (g) NLM101 - Normalized NIR image (Minnaert correction and 101 x 101 pixel window) (h) NLM201 - Normalized NIR image (Minnaert correction and 201 x 201 pixel window).

Table 9: Summary statistics for sample four.

Image	Min	Max	Mean	STD
NIR [a]	34.2789	153.6643	66.5968	15.6126
Cosine [b]	44.2103	458.2293	114.4305	36.6255
NLMG [c]	37.1499	184.4921	78.7519	17.4873
NLM3 [d]	35.4151	173.2128	72.7588	17.0640
NLM11 [e]	31.3988	196.1700	70.8735	19.5848
NLM21 [f]	34.5292	180.5494	71.7830	19.0859
NLM101 [g]	37.6109	239.3845	78.5853	20.9398
NLM201 [h]	93.0908	204.0349	78.4591	18.8894

[a]NIR - SPOT-3 NIR Image.
[b]Cosine -normalized NIR image (Cosine correction).
[c]NLMG - Normalized NIR image (Minnaert correction and global Minnaert constant).
[d]NLM3 - Normalized NIR image (Minnaert correction and land-cover stratification).
[e]Nlm11 - Normalized NIR image (Minnaert Correction and 11 x 11 pixel window).
[f]Nlm21 - Normalized NIR image (Minnaert Correction and 21 x 21 pixel window).
[g]Nlm101 - Normalized NIR image (Minnaert Correction and 101 x 101 pixel window).
[h]Nlm201 - Normalized NIR image (Minnaert Correction and 201 x 201 pixel window).

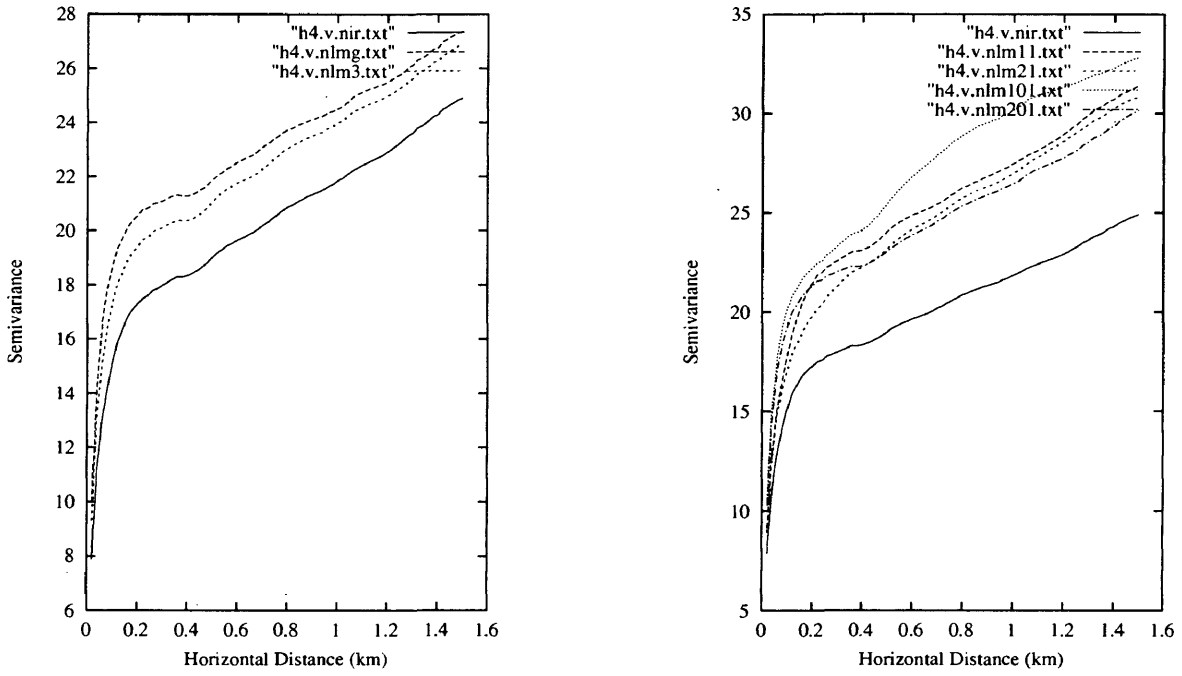

Figure 37: Two-dimensional semivariograms for sample four. (NIR) - SPOT3 NIR image, (NLM Global) - Normalized NIR image (Minnaert correction and global Minnaert constant), (NLM3) - Normalized NIR image (Minnaert correction and land-cover stratification), (NLM11) - Normalized NIR image (Minnaert correction and 11 x 11 pixel window), (NLM21) - Normalized NIR image (Minnaert correction and 21 x 21 pixel window), (NLM101) - Normalized NIR image (Minnaert correction and 101 x 101 pixel window), (NLM201) - Normalized NIR image (Minnaert correction and 201 x 201 pixel window).

6 Discussion

Addressing the problem of anisotropic reflectance in mountainous terrain is a notoriously difficult task. Consequently, investigators over the past twenty years have attempted to normalize satellite multispectral imagery, such that results represent an acceptable first-order approximation to solving the problem. Numerous researchers have indicated, however, that the full scope of the problem is computationally intractable, and that an approach using empirical modeling may produce acceptable results (Duguay and LeDrew, 1992; Hugli and Frei, 1983; Meyer et al., 1993).

It is important to note that the results obtained in this study and by Bishop and Colby (2002) indicate that this conclusion is not universally valid, and that results are highly dependent upon the complexity of the topography for a given area or region. In additon, the empirical approaches that are commonly used today do not address the issue of the irradiant flux, a factor which determines whether empirical modeling can effectively normalize satellite images. Furthermore, the influence of atmospheric effects on ARC have not been thoroughly studied, and it has yet to be determined how various ARC techniques will work on images recorded from the visible portions of the electromagnetic spectrum. These, and other issues, are specifically addressed for each ARC procedure evaluated in this study.

6.1 Cosine Correction

It is very clear from the visual and statistical analysis results, that the Cosine-correction method cannot be used for ARC of imagery in rugged terrain. These results have been

obtained by a variety of other investigators, indicating that this method frequently over-corrects, and produces high radiance values that are not representative of the reflectance characteristics of snow and other land-cover features. The problem is specifically associated with steep slopes, where the direct irradiance, as accounted for by $\cos i$, does not accurately model the surface irradiant flux (E_λ) for pixels. The procedure overestimates the surface radiance because it assumes Lambertian reflectance (this assumption is known to be invalid), and $\cos i$ does not accurately account for the magnitude of E_λ, as steep slopes have a higher irradiance because of the diffuse irradiance and adjacent terrain irradiance components (E_λ^d and E_λ^T respectively).

Other investigators have indicated that the Cosine-correction method may produce reasonable results where the topographic complexity is reduced, such that relief is minimal and slope angles are relatively low. Given these topographic conditions, it is possible that the procedure may produce reasonable first-order results and decrease the high spectral variance caused by the topography. The procedure, however, cannot account for variations in anisotropic reflectance caused by the land cover, and it is not clear how the procedure would work on imagery in the visible portion of the electromagnetic spectrum.

The SPOT-3 visible bands did not exhibit a strong topographic effect as did the NIR image. This is because the influence of the atmosphere masked the spectral variation caused by the topography. The atmospheric influence responsible for this is most likely the additive path-radiance component caused by atmospheric scattering. The significance of this additive term would increase with decreasing wavelength. It is also possible that there is an

atmospheric attenuation term that influences the spectral variance in the visible regions of the spectrum, as the variation in altitude is extreme over a very short distance. Given that the Cosine-correction method is solely based upon the utilization of $\cos i$, and there may not be a strong relationship between L and $\cos i$ in the visible regions of the spectrum, it is highly unlikely that the Cosine-correction method would effectively normalize imagery obtained in the visible portion of the spectrum. Therefore, based upon theoretical issues and empirical results, it can be safely concluded that the Cosine-correction method cannot be used for operational ARC in complex terrain.

It would, however, be interesting to evaluate the Cosine-correction method in complex terrain, if the other irradiance components were taken into consideration. An irradiance coefficient, α, could be generated and proportional to E_λ. This could be approximated by estimating the average hemispherical shielding of the topography, and generating a shielding coefficient that ranges from $0 - 1.0$ (α^d). The adjacent terrain irradiance could also be accounted for using a relative coefficient (α^T), such that α is computed as a rescaling of the sum of $\cos i$, α^d, and α^T, such that it ranges from $0.0 - 1.0$. This would be computationally intensive but would reduce the overcorrection associated with the use of only the direct irradiance component. More research to determine the feasibility of this approach seems warranted.

6.2 Minnaert Correction - Global k Value

The Minnaert-correction procedure appeared to produced superior results to the Cosine-correction method, as the magnitude of overcorrection was significantly reduced. Investigators have promoted this method for this reason, although attention to the results of the regression analysis have generally been ignored. High r^2 values are required to produce statistically significant k values that accurately characterize anisotropic reflectance. Unfortunately, most studies test the procedure on relatively small areas or regions where homogeneous land-cover characteristics exist, or in areas of relatively simple topographic conditions. In a less-complex mountain environment, we can expect the procedure to produce reasonable-to-excellent results, as homogeneous land-cover conditions will result in a high r^2 value, and moderate topographic conditions will permit $\cos i$ to reasonably estimate E_λ, thereby reducing overcorrection significantly.

The results clearly demonstrate that for complex mountain environments and large study areas, this implementation of the Minnaert-correction procedure will not work. Such conditions dictate that multiple land-cover classes and steep slopes will be encountered. One k value cannot accurately characterize anisotropic reflectance caused by multiple land-cover classes and unique topography. Given this situation, results of regression analysis will always produce statistically invalid k values, and overcorrection will occur where steep slopes exist. Consequently, the traditional approaches that investigators have been depending upon for diagnosing ARC (i.e. image interpretation and L-$\cos i$ scatterplots) cannot be used. Semivariogram analysis indicated that the results are inconsistent for different areas

of the image, even though the procedure appears to reduce spectral variation caused by the topography. Bishop and Colby (2002) found the same result and indicated this implementation cannot be used for operational ARC. Collectively these results indicate that land-cover variations must be accounted for. This would require the use of multiple k values, which would facilitate accurate characterization of the land cover influence on ARC, and solve the statistical problem of generating k values with associated high r^2 values.

Unfortunately, researchers and those who must use satellite imagery for resource assessment and management are arbitrarily selecting a k value that will appear to reduce spectral variation in multispectral data. This has occurred because usable software for ARC does not exist, and people are encouraged to this arbitrary usage by remote-sensing analysts not familiar with remote-sensing science. It is important to note that this approach is not scientifically valid, and results generated from such implementations produce spatially inconsistent results.

6.3 Minnaert Correction - Local k Values

Colby (1991) was the first to recognize that the Minnaert-correction procedure may produce better results if local land cover characteristics are taken into consideration. Testing of this assumption equates to generating multiple k values to characterize the local anisotropic-reflectance characteristics. Associated with generating multiple k values is the problem of scale, such that a particular scale of analysis must be chosen that enables characterization of land cover. The window-based approach to solving this problem enabled multiple scales

to be evaluated.

The results indicated that this approach cannot be used for operational ARC. The use of small windows for generating k values resulted in k values outside the permissible range, and in information compression. Such results will, of course, decrease the global variance, and this should not be confused with a reduction in variance caused by the topography. Statistical results were inconsistent, as small window sizes accurately account for land cover, but do not incorporate enough topographic variation to effectively reduce anisotropic reflectance. This was clearly demonstrated in Figures 22 and 23 where shallow slopes resulted in low r^2 values.

Conversely, large window sizes can account for topographic variation, but with increasing window size, multiple land-cover classes are included in the analysis. This dictates invalid statistical results, as the regression analysis cannot be used to accurately characterize reflectance variations caused by multiple land-cover classes. This resulted in spatially inconsistent results. The limitations of this implementation are related to the static window size. As the spatial complexity of the landscape changed, the scale of analysis was not permitted to be dynamically adjusted.

Although the results suggest that local land cover cannot be used effectively for ARC, one cannot discard the suggestion by Colby (1991), as it is possible to develop a dynamic stratification method that could automatically partition the spectral variation caused by land cover, and capture enough topographic variation to generate statistically valid results. The local stratification method would be dynamic, adjusting to changing landscape complexity,

thereby producing valid k values with high r^2 values. A local region-growing technique could be used to evaluate the topography and spectral variation in such a way as to partition the variance in n-dimensional space, and compute a k value based upon land-cover stratification. In this way, the land cover and topography would be accounted for. This would ensure statistically valid results. This would not address the overcorrection problem that is related to accounting for the irradiant flux. Additional research is required to establish a basis for adaptive analysis.

6.4 Minnaert Correction - Land Cover k Values

The Minnaert-correction procedure based upon land-cover stratification produced the most consistent results. Statistically valid k values were generated, and the procedure decreased spectral variation caused by the topography, while increasing spectral variation caused by land cover where appropriate. This result was obtained because land-cover conditions were accounted for and enough topographic variation was included in the regression analysis. The advantage of this approach is that the image can be further segmented to generate more classes, and more k values, which will produce better statistical results, as the variance is partitioned. It is unclear, however, whether more statistically valid k values would reduce or eliminate the overcorrection problem that occurred in some areas.

This implementation demonstrates the tremendous potential of the Minnaert-correction procedure for ARC. This implementation, however, does have a disadvantage in that it requires an accurate classification of the scene before ARC. This is potentially problematic,

as spectral variation caused by the topography can cause classification error. For operational ARC, the classification procedure would have to be automated and produce reliable results. The classification used in this study was generated using empirical procedures such as ratioing and thresholding, where the spectral variance caused by the topography can be reduced, and different ratios can be used to highlight different classes. Thus, this implementation of the Minnaert-correction procedure is a positive proof-of-concept that demonstrates this semi-empirical model can be used to effectively perform ARC. It can be significantly improved upon by making the procedure dynamically adaptive to the local complexity of the landscape, and by accounting for the other irradiance components so that overcorrection is not a problem. This should be a high research priority, as there is currently no method or software program that can effectively accomplish this on an operational basis.

An additional issue that must be addressed is that of diagnostic procedures for evaluating ARC results. It has been shown that visual interpretation, and L-cos i scatterplots are not effective diagnostic approaches for evaluating ARC results. Semivariogram analysis revealed that the ARC procedures altered the spatially dependent variance structure of the normalized images differently, depending upon the implementation option. Consequently, the visual appearance of a normalized image should never be used.

Numerous investigators have utilized the classification-accuracy approach as a means to evaluate ARC results (Colby, 1991; Colby and Keating, 1998). The assumption here is that if ARC improves the classification accuracy, compared to the use of the original data, then the ARC results are reasonable. This line-of-thinking is seriously flawed, and this

evaluation procedure does not truly evaluate the results of ARC. ARC is a radiometric calibration procedure to obtain accurate surface-radiance values for each pixel in the image. It is concerned with accounting for the irradiant and radiant flux caused by various environmental factors that influence the at-satellite recorded radiance. Consequently, evaluation of ARC results must focus on the magnitude of the normalized surface radiance, as well as on increasing or decreasing spectral variance given the landscape complexity. Classification results are not an appropriate diagnostic of ARC, as information compression can lead to improved classification results. Furthermore, numerous biophysical applications are not concerned with classification and instead focus on estimating biophysical parameters of the landscape. Effective radiometric calibration (i.e. ARC) is required for these applications.

7 Summary and Conclusion

Mountain environments are the result of complex interactions involving climate, tectonic and surface processes. Geoscientists are interested in studying these interactions by using topographic information generated from remotely sensed data, and by utilizing satellite imagery that can help them study the spatial and temporal dynamics of the landscape. Furthermore, it is essential that scientists be able to monitor the environment and detect landscape changes to determine whether environmental change is the result of anthropogenic factors. Similarly, it is essential that scientists be able to assess natural change in order to understand the Earth's complex dynamic systems. Mountain environments represent dynamic and sensitive systems that need to be systematically monitored.

Advanced sensors are required to generate new multispectral imagery over mountain environments from unique regions of the electromagnetic spectrum. With the advent of missions such as Landsat-7 and Terra, scientists now have a tremendous volume of mulitemporal and multispectral data that can be used to study the landscape and monitor change. Unfortunately, the government has appropriated more resources towards the development of hardware technology than on scientific research and development of information technology to address a variety of remote sensing science and technology issues. Consequently, Earth scientists are struggling with the analysis of multispectral data, especially in extracting reliable information from imagery over rugged terrain.

The problem of anisotropic-reflectance correction has yet to be adequately addressed so that scientists can study mountain environments using remotely sensed data. The topog-

raphy influences the irradiant and radiant flux, such that the at-satellite recorded radiance exhibits variation that is related to a variety of environmental variables that are inter-related in complex non-linear ways. Consequently, image radiance is highly variable, depending upon the topography, atmosphere and landscape complexity. Therefore, the *topographic effect* is usually present in satellite imagery.

The issue is one of anisotropic-reflectance correction, as the topography and land cover causes the irradiant and radiant flux to spatially vary throughout a scene. Numerous investigators have attempted to address this problem without much success. Consequently, the overall objective of this research was to evaluate various normalization procedures in one of the most rugged landscapes on the planet, the western Himalaya. Specifically, the objectives were to evaluate the Cosine-correction method and various implementations of the Minnaert-correction procedure, as previous research has indicated their potential to address the issue of ARC in rugged terrain.

The first hypothesis stated that the Cosine-correction method would not work at Nanga Parbat, or in other complex mountain environments because these surfaces do not exhibit isotropic reflectance. The widely utilized Cosine-correction method did a poor job of normalizing the SPOT HRV NIR image. Statistical and semivariogram analyses confirmed that extreme radiance values were produced, which increased the spatially dependent variance at all lag distances. These results were similar to results by a variety of investigators who have indicated that the method fails because the other irradiance terms are not accounted for. It should also be recognized that the method does not account for anisotropic

reflectance caused by land cover. It assumes Lambertian reflectance, which is known to be invalid in rugged mountain terrain. Consequently, the first hypothesis must be accepted.

The utility of the Cosine-correction method for operational ARC, however, should not be totally discarded until it is evaluated with respect to a more appropriate irradiance coefficient. Topographic analysis of the landscape could be used to produce a proxy for the diffuse-skylight irradiance component which could be effectively integrated with $\cos i$ to produce a more accurate irradiance coefficient. If we assume that the adjacent terrain irradiance term has less of an influence on E_λ than E_λ^d does, then we can sum and re-scale the irradiance coefficient, and re-evaluate the utility of the cosine correction method to determine what degree the assumption of Lambertian reflectance can be used as a first-order approximation for ARC. Furthermore, more research is required to first determine what the magnitude of the influence of the different irradiance components are in relation to the topographic complexity, and to determine if topographic analysis of the landscape can be used to accurately generate an irradiance coefficient as a proxy for E_λ. Successful implementation of this research would address the ubiquitous problem of the over correction issue in ARC.

The results indicate that the second hypothesis must be accepted, which indicated that the use of one k value cannot be used when using the Minnaert-correction approach for ARC. This implementation did not effectively characterize anisotropic reflectance.

Unfortunately, many people have utilized this approach, because it appears to reduce the spectral variance caused by the topography. Furthermore, software tools enable scientists,

planners, and managers to arbitrarily select a k value and normalize the imagery. This approach should not be utilized, as it produces erroneous results and requires statistically valid regression results in order to work. The approach should never be used unless the study area is homogeneous in terms of land-cover characteristics, and regression results are valid (r^2 is high).

Colby (1991) indicated that the utility of local land-cover information may significantly improve the results of ARC, as the influence of land cover on anisotropic reflectance would be accounted for. This was one of the objectives of this study, and it was formalized and tested by using the window-stratification approach to calculating a local k value for each pixel. The results indicated that we must accept the third hypothesis, which indicated that this approach cannot be used for effective ARC in complex mountain environments. The approach produced inconsistent results in terms of valid parameters from regression. For smaller window sizes, invalid k values were produced, and low r^2 values were generated where topographic variation was not adequately sampled. For larger window sizes, topographic variation was adequately sampled, but the inclusion of multiple land-cover classes produced low r^2 values, which resulted in k values not adequately characterizing the influence of land cover.

The acceptance of the third hypothesis, however, does not prove that the inclusion of local-land cover information does not improve ARC results. The problem is with the static window-based implementation approach. Given this implementation, an optimal analysis scale must be selected so that an appropriate amount of topographic variation is sampled.

This approach did not work because as the window size increased, multiple land-cover classes were included in the analysis, and an appropriate window size can only be determined based upon the complexity of the landscape. Furthermore, the static approach did not account for the changing complexity of the landscape over the large area that was analyzed. Although the results indicated that this approach cannot be used for operational ARC, it does demonstrate that if land-cover information can be dynamically accounted for, land cover information should improve ARC results, verifying the suggestion of Colby (1991).

The fourth hypothesis stated that a dynamic-landscape analysis procedure would account for spectral and topographic variation such that image normalization would result in relatively high spectral variation. This must be qualified so that it does not include variance that is the result of lower signal-to-noise ratio and it must also be associated with valid Minnaert constants and statistically significant r^2 values. The results clearly demonstrated that land-cover stratification is an effective approach for ARC. Consequently, the fourth hypothesis must be accepted. By simply increasing the number of land-cover classes that are taken into consideration, the variance is further partitioned, thereby producing even higher $r^2 values$, and k values which better characterize anisotropic reflectance. The potential problem with this implementation approach is that classification is required before ARC.

The results from the window-based and land-cover stratification approaches are effectively the same implementation of the Minnaert-correction procedure. It is necessary to

evaluate the topographic complexity and the radiance variation around each pixel so an adaptive stratification procedure would ensure the generation of valid parameters from regression. This is a statistical solution to the problem, and additional research would be required regarding topographic complexity metrics for stratification. This would, however, represent a solution to addressing the problems of the Minnaert-correction procedure, and may have significant value for operational ARC.

The results clearly show the potential of the Minnaert-correction procedure for ARC if the statistical problem of generating valid k values is addressed. This research, however, did not address the problem of over correction which was found in every implementation of the Minnaert correction procedure. Clearly, in rugged terrain, the other irradiance components must be considered. As previously mentioned, it is strongly suspected that substituting an irradiance coefficient for $\cos i$ would address the problem of over correction and result in better k values. This research is sorely needed as it would comprehensively evaluate the Minnaert correction procedure for its utility to be used for operational ARC.

This research has also demonstrated that image interpretation cannot be used to evaluate ARC results. ARC methods alter the spatially dependent variance structure in imagery, and can increase or decrease variance depending upon the complexity of the landscape. Special care needs to be exercised when evaluating ARC results, and it is recommended that visual interpretation and classification-accuracy assessment not be used. The nature of the problem is radiometric calibration. Improving classification results is not an indication that surface radiance values have been correctly normalized, as linear information compression

improves classification results. It is highly recommended that semivariogram analysis be used as a diagnostic tool to determine the effectiveness of ARC when field measurements of the irradiant and radiant flux are not available. In this way, the altered spatially dependent variance structure can be compared to the original imagery.

Finally, this research has not evaluated the utility of ARC on imagery obtained from the visible portion of the electromagnetic spectrum. The SPOT imagery from the visible portions of the spectrum did not exhibit the topographic effect to the same degree as the NIR band, as the additive influence of atmospheric scattering masked the topographic effect. It is suspected that the Minnaert-correction procedure would not work very well on these images, as the variance structure is more related to land-cover and atmospheric conditions. More research is required to determine what influence the atmosphere has on ARC methods. This is especially important because radiation transfer is governed by the complex interaction of radiation with the atmosphere and the topography.

References

Allen, M., Delworth, T., Scott, P., Mitchell, J., and Schnur, R., 2000. Quantifying the uncertainty in forecasts of anthropogenic climate change. *Nature*, **407**, 617–620.

Allen, T. and Walsh, S., 1996. Spatial and compositional pattern of alpine treeline, Glacier National Park, Montana. *Photogrammetric Engineering and Remote Sensing*, **62**, 11, 1261–1268.

Bishop, M. P. and Colby, J. D., 2002. Anisotropic reflectance correction of SPOT-3 HRV imagery. *International Journal of Remote Sensing*.

Bishop, M. P., Shroder, J. F., Sloan, V., Copland, L., and Colby, J., 1998a. Remote sensing and GIS technology for studying lithospheric processes in a mountain environment. *Geocarto International*, **13**, 4, 75–87.

Bishop, M. P. and Shroder, Jr., J. F., 2000. Remote sensing and geomorphometric assessment of topographic complexity and erosion dynamics in the Nanga Parbat massif. In Khan et al. (2000), pages 181–200.

Bishop, M. P., Shroder, Jr., J. F., Hickman, B. L., and Copland, L., 1998b. Scale dependent analysis of satellite imagery for characterization of glacier surfaces in the Karakoram Himalaya. *Geomorphology*, **21**, 217–232.

Bishop, M. P., Shroder, Jr., J. F., and Ward, J. L., 1995. SPOT multispectral analysis for producing supraglacial debris-load estimates for Batura Glacier, Pakistan. *Geocarto International*, **10**, 4, 81–90.

Brozovik, N., Burbank, D. W., and Meigs, A. J., 1997. Climatic limits on landscape development in the northwestern Himalaya. *Science*, **276**, 571–574.

Burbank, D., Leland, J., Fielding, E., Anderson, R. S., Brozovik, N., Reid, M. R., and Duncan, C., 1996. Bedrock incision, rock uplift and threshold hillslopes in the northwestern Himalaya. *Nature*, **379**, 505–510.

Chavez, Jr., P. S., 1996. Image-based atmospheric corrections – Revisited and improved. *Photogrammetric Engineering and Remote Sensing*, **62**, 9, 1025–1036.

Civco, D., 1989. Topographic normalization of Landsat Thematic Mapper digital imagery. *Photogrammetric Engineering and Remote Sensing*, **55**, 9, 1303–1309.

Colby, J., 1991. Topographic normalization in rugged terrain. *Photogrammetric Engineering and Remote Sensing*, **57**, 5, 531–537.

Colby, J. D. and Keating, P. L., 1998. Land cover classification using Landsat TM imagery in the tropical highlands: The influence of anisotropic reflectance. *International Journal of Remote Sensing*, **19**, 8, 1459–1500.

Conese, C., Gilabert, M., Maselli, F., and Bottai, L., 1993a. Topographic normalization of TM scenes through the use on an atmospheric correction method and digital terrain models. *Photogrammetric Engineering and Remote Sensing*, **59**, 12, 1745–1753.

Conese, C., Maracchi, G., and Maselli, F., 1993b. Improvement in maximum likelihood classification performance on highly rugged terrain using principal components analysis. *International Journal of Remote Sensing*, **14**, 7, 1371–1382.

Davis, F. W., Quattrochi, D. A., Kidd, M. K., Lam, N. S. N., Walsh, S. J., Michaelsen, J. C., Franklin, J., Stow, D. A., Johannse, C. J., and Johnston, C. A., 1991. Environmental analysis using integrated GIS and remotely sensed data: Some research needs and priorities. *Photogrammetric Engineering and Remote Sensing*, **57**, 6, 689–697.

Dehn, M. and Buma, J., 1999. Modeling future landslide activity based on general circulation models. *Geomorphology*, **30**, 1-2, 175–187.

Delworth, T. and Knutson, T., 2000. Simulation of early 20th century global warming. *Science*, **287**, 5461, 2246–2250.

Dowdeswell, J., 1995. Glaciers in the high Arctic and recent environmental change. *Philosophical Transactions - Royal Society of London*, **352**, 1699, 321–334.

Dowdeswell, J., Harrison, W., Holmlund, P., Jania, J., Koerner, R., Lefauconnier, B., Ommanney, C., Thomas, R., Hagen, J., Bjornsson, H., and Glazovsky, A., 1997. The mass balance of circum-Arctic glaciers and recent climate change. *Quaternary Research*, **48**, 1, 1–14.

Dozier, J., 1980. A clear-sky spectral solar radiation model for snow-covered mountainous terrain. *Water Resources Research*, **16**, 4, 709–718.

Dozier, J. and Frew, J., 1990. Rapid calculation of terrain parameters for radiation modeling from digital elevation data. *IEEE Transactions on Geoscience and Remote Sensing*, **28**, 5, 963–969.

Duguay, C. and LeDrew, E., 1992. Estimating surface reflectance and albedo from Landsat-5 Thematic Mapper over rugged terrain. *Photogrammetric Engineering and Remote Sensing*, **58**, 5, 551–558.

Dyurgerov, M. and Meier, M., 1999. Year-to-year fluctuations of global mass balance of small glaciers and their contribution to sea-level changes. *Arctic and Alpine Research*, **29**, 4, 392–402.

Ekstrand, S., 1996. Landsat TM-based forest damage assessment: Correction for topographic effects. *Photogrammetric Engineering and Remote Sensing*, **62**, 2, 151–161.

Gemmel, F., 1998. An investigation of terrain effects on the inversion of a forest reflectance model. *Remote Sensing of the Environment*, **65**, 155–169.

Giles, P. T., 2001. Remote sensing and cast shadows in mountainous terrain. *Photogrammetric Engineering and Remote Sensing*, **67**, 7, 833–839.

Goward, S. N. and Williams, D. L., 1997. Landsat and Earth systems science: Development of terrestrial monitoring. *Photogrammetric Engineering and Remote Sensing*, **63**, 7, 887–900.

Greuell, W. and de Wildt, M., 1999. Anisotropic reflection by melting glacier ice: Measurements and parametrizations in Landsat TM bands 2 and 4. *Remote Sensing of Environment*, **70**, 265–277.

Gu, D. and Gillespie, A., 1998. Topographic normalization of Landsat TM images of forest based on subpixel sun-canopy-sensor geometry. *Remote Sensing of the Environment*, **64**, 166–175.

Hall, D. K., Chang, A. T. C., Foster, J. L., Benson, C. S., and Kovalick, W. M., 1989. Comparison of In-Situ and Landsat derived reflectance of Alaskan glaciers. *Remote Sensing of the Environment*, **28**, 23–31.

Hugli, H. and Frei, W., 1983. Understanding anisotropic reflectance in mountainous terrain. *Photogrammetric Engineering and Remote Sensing*, **49**, 5, 671–683.

Jin, Z. and Simpson, J., 1999. Bidirectional anisotropic reflectance of snow and sea ice in AVHRR channel 1 and 2 spectral regions-part I: Theoretical analysis. *IEEE Transactions on Geoscience and Remote Sensing*, **37**, 1, 543–554.

Khan, M. A., Treloar, P. J., Searle, M. P., and Jan, M. Q., eds., 2000. *Tectonics of the Nanga Parbat Syntaxis and the Western Himalaya*. Number 170 in Special Publication. Geological Society, London.

Kimes, D. S. and Kirchner, J. A., 1981. Modeling the effects of various radiant transfers in mountainous terrain on sensor response. *IEEE Trans. on Geoscience and Remote Sensing*, **19**, 2, 100–108.

Kirilenko, A., Belotelov, N., and Bogatyrev, B., 2000. Global model of vegetation migration: Incorporation of climatic variability. *Ecological Modelling*, **132**, 1-2, 125–133.

Kowalik, W. S., Lyon, R. J. P., and Switzer, P., 1983. The effects of additive radiance terms on ratios of Landsat data. *Photogrammetric Engineering and Remote Sensing*, **49**, 5, 659–669.

Latif, M., Roeckner, E., Mikolajewicz, U., and Voss, R., 2000. Tropical stabilazation of the thermohaline circulation in a greenhouse warming simulation. *Journal of Climate*, **13**, 11, 1809–1813.

Leung, L. and Wigmosta, M., 1999. Potential climate change impacts on mountain watersheds in the pacific northwest. *Journal of the American Water Resources Association*, **35**, 6, 1463–1471.

Levi, S., Jonathan, A., Brovkin, V., and Pollard, D., 1999. On the stability of the high-latitude climate-vegetation system in a coupled atmosphere-biosphere model. *Global Ecology and Biogeography*, **8**, 6, 489–500.

MacFarlane, N. and Robinson, I., 1984. Atmospheric correction of Landsat MSS data for a multidate suspended sediment algorithm. *Journal of Remote Sensing*, **5**, 3, 561–576.

Meyer, P., Itten, K., Kellenberger, T., Sandmeier, S., and Sandmeier, R., 1993. Radiometric corrections of topographically induced effects on Landsat TM data in alpine environment. *Journal of Remote Sensing*, **48**, 4, 17–28.

Osterhus, S. and Gammelsrod, T., 1999. The abyss of the Nordic Seas is warming. *Journal of Climate*, **12**, 11, 3297–3304.

Phillips, W. M., Sloan, V. F., Shroder, Jr., J. F., Sharma, P., Clarke, M. L., and Rendell, H. M., 2000. Asynchronous glaciation at Nanga Parbat, northwestern Himalaya Mountains, Pakistan. *Geology*, **28**, 431–434.

Price, M. F. and Heywood, D. I., 1994. *Mountain Environments and Geographic Information Systems*. Taylor and Francis, London.

Proy, C., Tanre, D., and Deschamps, P. Y., 1989. Evaluation of topographic effects in remotely sensed data. *Remote Sensing of the Environment*, **30**, 21–32.

Przybylak, R., 2000. Temporal and spatial variation of surface air temperature over the period of instrumental observations in the arctic. *International Journal of Climatology*, **20**, 6, 587–614.

Richter, R., 1997. Correction of atmospheric and topographic effects for high spatial resolution satellite imagery. *International Journal of Remote Sensing*, **18**, 5, 1099–1111.

Saraf, A., 1998. IRS-LISS-II improves geological mapping in the Himalayas. *International Journal of Remote Sensing*, **19**, 12, 2239–2243.

Schneider, D. A., Edwards, M. A., Kidd, W. S. F., Khan, M. A., Seeber, L., and Zeitler, P. K., 1999. Tectonics of Nanga Parbat, western Himalaya: Synkinematic plutonism within the doubly vergent shear zones of a crustal-scale pop-up structure. *Geology*, **27**, 999–1002.

Shroder, J. F. and Bishop, M. P., 1998. Mass movement in the himalaya: New insights and research directions. *Geomorphology*, **26**, 13–35.

Shroder, J. F., Scheppy, R., and Bishop, M. P., 1999. Denudation of small alpine basins, Nanga Parbat Himalaya, Pakistan. *Arctic, Antarctic, and Alpine Research*, **31**, 2, 121–127.

Shroder Jr., J. F. and Bishop, M. P., 2000. Unroofing of the Nanga Parbat Himalaya. In Khan, M. A., Treloar, P. J., Searle, M. P., and Jan, M. Q., eds., *Tectonics of the Nanga Parbat Syntaxis and the Western Himalaya*, volume 170 of *Special Publications*, pages 163–179. Geological Society, London.

Smith, J., Lin, T., and Ranson, K., 1980. The Lambertian assumption and Landsat data. *Photogrammetric Engineering and Remote Sensing*, **46**, 9, 1183–1189.

Teillet, P., Guindon, B., and Goodenough, D., 1982. On the slope-aspect correction of multispectral scanner data. *Canadian Journal of Remote Sensing*, **8**, 2, 84–106.

Vinnikov, K., Parkinson, C., Cavalieri, D., Mitchell, J., Garrett, D., Zakharov, V., Robock, A., Stouffer, R., and Walsh, J., 1999. Global warming and northern hemisphere sea ice extent. *Science*, **286**, 5446, 1934–1937.

Watterson, I., 2000. Interpretation of simulated global warming using a simple model. *Journal of Climate*, **13**, 1, 202–215.

Wild, M. and Ohmura, A., 2000. Change in mass balance of polar ice sheets and sea level from high-resolution GCM simulations of greenhouse warming. *Annals of Glaciology*, **30**, 197–203.

Wu, X., Budd, W., and Jacka, T., 1999. Simulations fo southern hemisphere warming and Antarctic sea-ice changes using global climate models. *Annals of Glaciology*, **29**, 61–65.

Yang, C. and Vidal, A., 1990. Combination of digital elevation models with SPOT-1 HRV multispectral imagery for reflectance factor mapping. *Remote Sensing of the Environment*, **32**, 35–45.

Yool, S., Starr, J., Estes, J., Botkin, D., Eckhardt, D., and Davis, F., 1986. Performance analysis of image processing algorithms for classification of natural vegetation in the mountains of Southern California. *International Journal of Remote Sensing*, **7**, 5, 683–702.

Zeitler, P. K., Meltzer, A. S., Koons, P. O., Craw, D., Hallet, B., Chamberlain, C. P., Kidd, W. S., Park, S. K., Seeber, L., Bishop, M. P., and Shroder, Jr., J. F., 2001. Erosion, Himalayan geodynamics, and the geomorphology of metamorphism. *GSA Today*, **11**, 4–8.